

Maintenance of R-loop structures by phosphorylated hTERT preserves genome integrity

Received: 18 July 2023

Accepted: 23 April 2024

Published online: 28 May 2024

 Check for updates

Mitsuhiro Machitani ^{1,10}, Akira Nomura ^{1,2,10}, Taro Yamashita ³, Mami Yasukawa ¹, Saori Ueki¹, Ken-Ichi Fujita¹, Toshihide Ueno ⁴, Akio Yamashita ⁵, Yoshikazu Tanzawa², Masahiko Watanabe ², Toshiyasu Taniguchi⁶, Noriko Saitoh ⁷, Shuichi Kaneko ³, Yukinari Kato ^{8,9}, Hiroyuki Mano ⁴ & Kenkichi Masutomi ¹ 

As aberrant accumulation of RNA–DNA hybrids (R-loops) causes DNA damage and genome instability, cells express regulators of R-loop structures. Here we report that RNA-dependent RNA polymerase (RdRP) activity of human telomerase reverse transcriptase (hTERT) regulates R-loop formation. We found that the phosphorylated form of hTERT (p-hTERT) exhibits RdRP activity in nuclear speckles both in telomerase-positive cells and telomerase-negative cells with alternative lengthening of telomeres (ALT) activity. The p-hTERT did not associate with telomerase RNA component in nuclear speckles but, instead, with TERRA RNAs to resolve R-loops. Targeting of the *TERT* gene in ALT cells ablated RdRP activity and impaired tumour growth. Using a genome-scale CRISPR loss-of-function screen, we identified Fanconi anaemia/BRCA genes as synthetic lethal partners of hTERT RdRP. Inactivation of RdRP and Fanconi anaemia/BRCA genes caused accumulation of R-loop structures and DNA damage. These findings indicate that RdRP activity of p-hTERT guards against genome instability by removing R-loop structures.

Cells counteract the induction of genome instability through DNA repair facilitated by DNA damage response (DDR), which recruits various DDR effectors to DNA lesions for DNA repair (reviewed in ref. 1). Such genome instability also associates with abnormal genome structures. An R-loop is a three-stranded nucleic acid structure containing RNA–DNA hybrids, formed along with transcriptional elongation due to annealing of the nascent RNA strand with the template DNA strand. R-loops enrich in specific regions such as transcription initiation and termination sites, DNA damage sites and telomere regions².

Accumulation of aberrant R-loops induces destabilization of genome structure and inhibition of transcript maturation, causing DNA damage and cell death. To prevent such adverse effects by accumulation of R-loop structures, cells express regulators. For example, RNase H family proteins digest the RNA strand of R-loops^{3,4}, and the helicase senataxin (SETX)⁵ and DEAH box helicase 9 (DHX9)⁶ unwind R-loop structures.

Telomere structures also maintain genome stability by protecting the ends of chromosomes (reviewed in ref. 7). Most cancers maintain telomeres relying on upregulation of telomerase, which consists of a

¹Division of Cancer Stem Cell, National Cancer Center Research Institute, Tokyo, Japan. ²Department of Orthopaedic Surgery, Surgical Science, Tokai University School of Medicine, Isehara, Japan. ³Department of Gastroenterology, Kanazawa University Graduate School of Medical Sciences, Kanazawa, Japan. ⁴Division of Cellular Signaling, National Cancer Center Research Institute, Tokyo, Japan. ⁵Department of Investigative Medicine, University of the Ryukyus Graduate School of Medicine, Nakagami, Japan. ⁶Department of Molecular Life Science, Tokai University School of Medicine, Isehara, Japan. ⁷Division of Cancer Biology, The Cancer Institute of JFCR, Tokyo, Japan. ⁸Department of Antibody Drug Development, Tohoku University Graduate School of Medicine, Sendai, Japan. ⁹Department of Molecular Pharmacology, Tohoku University Graduate School of Medicine, Sendai, Japan. ¹⁰These authors contributed equally: Mitsuhiro Machitani, Akira Nomura. ✉ e-mail: kmasutom@ncc.go.jp

catalytic component hTERT^{8–10} and a template RNA of human telomerase RNA component (hTERC)¹¹. Although telomerase plays an essential role in maintaining telomeres, previous studies have reported that hTERT has non-canonical functions beyond telomere maintenance^{12,13}. We reported previously that hTERT has RdRP activity, which functions to transcribe an antisense RNA from a template RNA^{14,15}. Phosphorylation of hTERT at threonine 249 by the serine/threonine kinase CDK1 is a key mechanism to regulate RdRP activity¹⁶. The synthesis of antisense RNAs by the RdRP activity of hTERT negatively regulates various target RNA levels such as transcripts of tumour suppressor genes, eventually leading to tumour formation^{14–16}. In addition, we detected high levels of p-hTERT expression in aggressive cancers with poor prognosis including lung, pancreatic and liver cancers¹⁷.

Here we found a functional role of the RdRP reaction by hTERT in R-loop regulation and maintenance of genome stability. We found that p-hTERT localizes in nuclear speckles (NSs) but not telomeres. It associates with telomeric repeat-containing (TERRA) noncoding RNAs transcribed from subtelomeric regions and dissolves R-loop structures, indicating that RdRP activity of hTERT functions to guard against genome instability through removal of R-loop structures.

Results

ALT cells express a phosphorylated form of hTERT

To examine p-hTERT expression, we performed indirect immunofluorescence (IIF) staining using previously described anti-p-hTERT mAbs (TpMab-1 and TpMab-3)^{16,17} and observed the specific signal of p-hTERT in the nuclei of several immortal cell lines (Fig. 1a,b). We included a subset of cancer cells that retain telomere length by a telomerase-independent mechanism based on homologous recombination, called ALT. We found that p-hTERT was also detected in ALT cells (U2OS, VA-13 and Saos-2 cells), although these cells lack telomerase activity, in agreement with previous reports (Fig. 1a,b). When we suppressed hTERT expression using siRNAs specific for hTERT (siTERT#1 and #2), the p-hTERT signals were diminished (Fig. 1c). To confirm the phosphorylation specificity of these signals, we treated HeLa and U2OS cells with an inhibitor of CDK1 that catalyses phosphorylation of hTERT at threonine 249 (ref. 16). Treatment with CDK1 inhibitor RO-3306 diminished the specific signal of p-hTERT in these cells (Fig. 1d). In addition, we generated another mAb specific for p-hTERT (clone TpMab-35) and observed identical signals of p-hTERT in all cell lines (Extended Data Fig. 1a–c). To further confirm the expression of hTERT in ALT cells by semi-quantitative and quantitative RT-PCR (qRT-PCR) analyses, we optimized conditions to identify hTERT expression (Extended Data Fig. 1d–g) using primers specific for exons 15 and 16, and detected hTERT mRNA in U2OS, VA-13 and Saos-2 cells (approximately one-third versus that in HeLa cells; Fig. 1e).

Next, we examined p-hTERT expression in mitotic ALT cells, because hTERT is enriched during mitosis in telomerase-positive cells^{15,18}. When we synchronized ALT cells in mitotic phase, we found that mitotic U2OS cells expressed high levels of p-hTERT spreading throughout the whole cell (Fig. 1f). We further investigated the expression of p-hTERT in ALT cells using lysates of mitotic cells synchronized by treatment with nocodazole. Because it is difficult to detect endogenous hTERT, we performed immunoprecipitation (IP)

with an anti-hTERT mAb (clone 10E9-2) followed by immunoblotting (IB). Consistent with the IIF images, we observed endogenous hTERT (Fig. 1g) and p-hTERT (Fig. 1h) in U2OS, VA-13 and Saos-2 cells synchronized in the mitotic phase. Another mAb specific for p-hTERT (clone TpMab-35) also detected p-hTERT signals in mitotic U2OS cells (Extended Data Fig. 1h,i). These observations suggest that synchronization in the mitotic phase facilitated detection of p-hTERT in ALT cells. In addition, knockdown of hTERT eliminated the hTERT (Fig. 1i) and p-hTERT (Fig. 1j) signals, indicating that these signals are specific for hTERT and p-hTERT. Moreover, we confirmed that treatment with the CDK1 inhibitor RO-3306 ablated p-hTERT signals (Fig. 1k). These findings indicate that p-hTERT is present even in ALT cells lacking telomerase activity.

p-hTERT in ALT cells exhibits RdRP activity

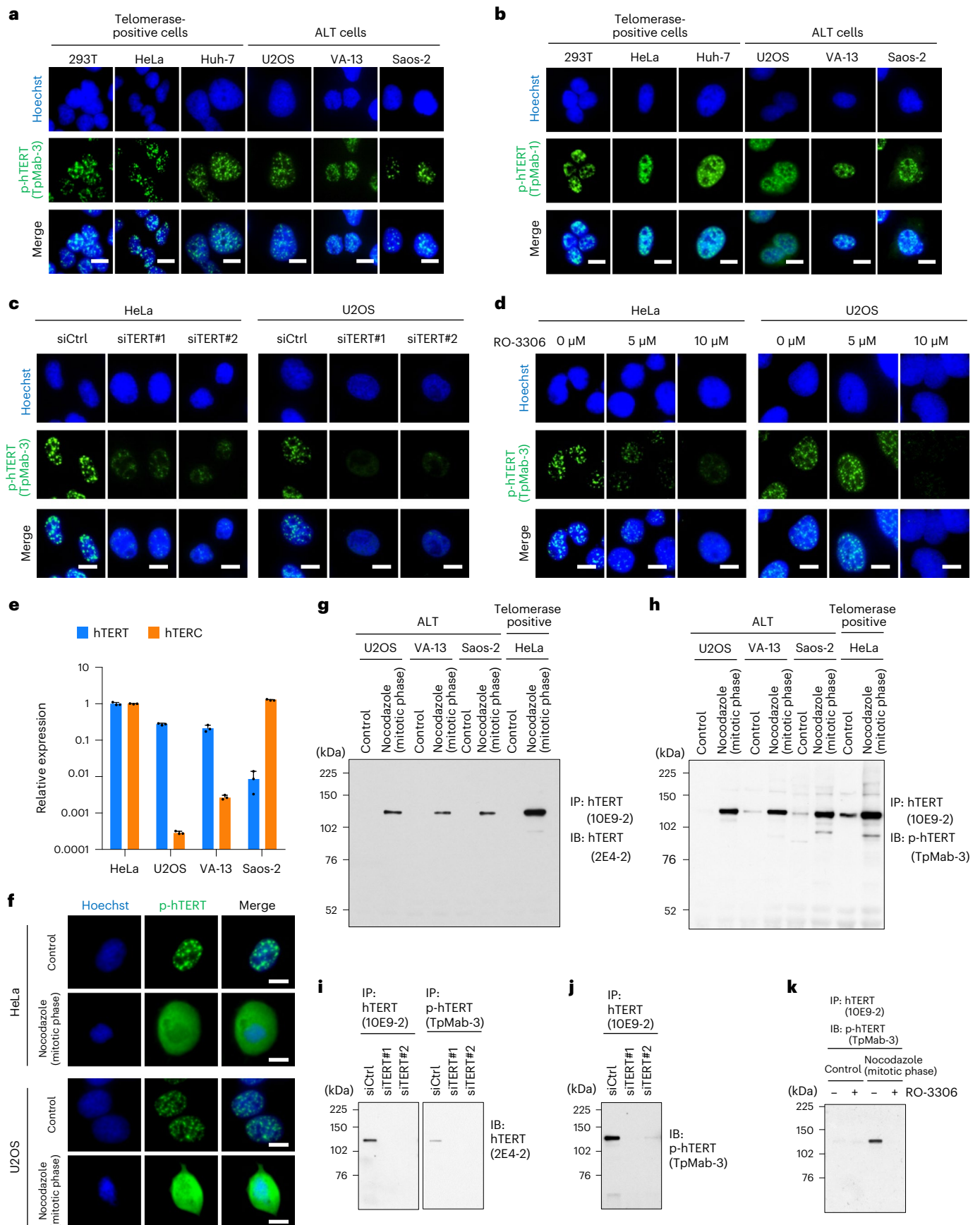
In agreement with previous reports^{19,20}, we confirmed lower but detectable levels of hTERC in addition to hTERT mRNA in ALT cells (Fig. 1e), which is essential for telomerase activity. To assess telomerase and RdRP activities of hTERT in ALT cells, we isolated hTERT immune complex with hTERT-specific antibodies from ALT cells, and subsequently performed a direct telomerase assay and RdRP assay. We confirmed that IP with the hTERT-specific antibodies recovered endogenous hTERT proteins (Extended Data Fig. 2a). Although the hTERT immune complex isolated from telomerase-positive 293T cell lysate with the anti-hTERT antibodies (10E9-2 and abx120550; refs. 21,22) exhibited detectable level of telomerase activities, the p-hTERT immune complex isolated with the p-hTERT-specific antibody (clone TpMab-3) exhibited no telomerase activity (Fig. 2a). In addition, we found that p-hTERT does not associate with hTERC (Fig. 2b), suggesting that p-hTERT does not form a complex with hTERC and thus lacks telomerase activity.

Consistent with several studies^{23–25}, we ascertained that ALT cells exhibited no telomerase activity (Fig. 2a and Extended Data Fig. 2b). We found that hTERT in ALT cells does not associate with hTERC (Fig. 2c and Extended Data Fig. 2c), even if ALT cells express both hTERT and hTERC (Fig. 1e). These results suggest that hTERT does not form a complex with hTERC in ALT cells, explaining the previously reported lack of telomerase activity in ALT cells. By contrast, we found that p-hTERT isolated from these ALT cells exhibited RdRP activity (Fig. 2d,e). In addition, knockdown of hTERT (Fig. 2f) and inhibition of hTERT phosphorylation with the CDK1 inhibitor RO-3306 (Fig. 2g) decreased the RdRP activity of hTERT in mitotic U2OS cells. We previously verified the RdRP activity with a recombinant hTERT (rhTERT) protein partially purified from *E. coli*¹⁴. Consistent with the previous finding, we confirmed that not only hTERT immunoprecipitated from cells but also rhTERT expressed by a baculovirus expression system exhibits RdRP activity (Extended Data Fig. 2d). Because the recombinant protein partially purified from a non-mammalian system does not associate with other mammalian factors, these observations suggest that hTERT itself, but not a protein that associates with hTERT, possesses RdRP activity. Together, these findings indicate that p-hTERT exhibits RdRP activity in a hTERC-independent manner instead of telomerase activity in ALT cells.

Since various hTERT alternative splicing (AS) variants (such as α , β , γ , $\Delta 2$ and $\Delta 4$ -13 variants) have been identified even in ALT cells^{26–28}, we

Fig. 1 | Expression of phosphorylated hTERT proteins in ALT cells. a, b, IIF imaging of p-hTERT. Telomerase-positive cell lines (293T, HeLa and Huh-7 cells) and ALT cell lines (U2OS, VA-13 and Saos-2 cells) were immunostained with anti-p-hTERT mouse mAbs (TpMab-3 (a) and TpMab-1 (b)). Scale bars, 10 μ m. **c, d**, IIF imaging of p-hTERT (TpMab-3) in HeLa and U2OS cells treated with hTERT siRNAs (c) or a CDK1 inhibitor (RO-3306; d). Scale bars, 10 μ m. **e**, hTERT mRNA and hTERC expression levels in telomerase-positive HeLa and ALT (U2OS, VA-13 and Saos-2) cells, assessed by quantitative RT-PCR analysis using hTERT_ex15-16 primer pairs ($n = 3$ independent experiments per group).

Data are presented as mean \pm s.d. **f**, Detection of p-hTERT (TpMab-3) signals in HeLa and U2OS cells synchronized in mitosis with nocodazole. Scale bars, 10 μ m. **g, h**, Detection of endogenous hTERT (2E4-2; **g**) and p-hTERT (TpMab-3; **h**) by IP and the subsequent IB from the cells with nocodazole treatment. **i–k**, IP-IB of endogenous hTERT and p-hTERT proteins in U2OS cells with hTERT knockdown or CDK1 inhibitor (RO-3306) treatment. The cells were treated with nocodazole. Experiments were repeated three times (a, b, d, f–k) or twice (c) with similar results. Numerical source data and unprocessed blots are available as source data.



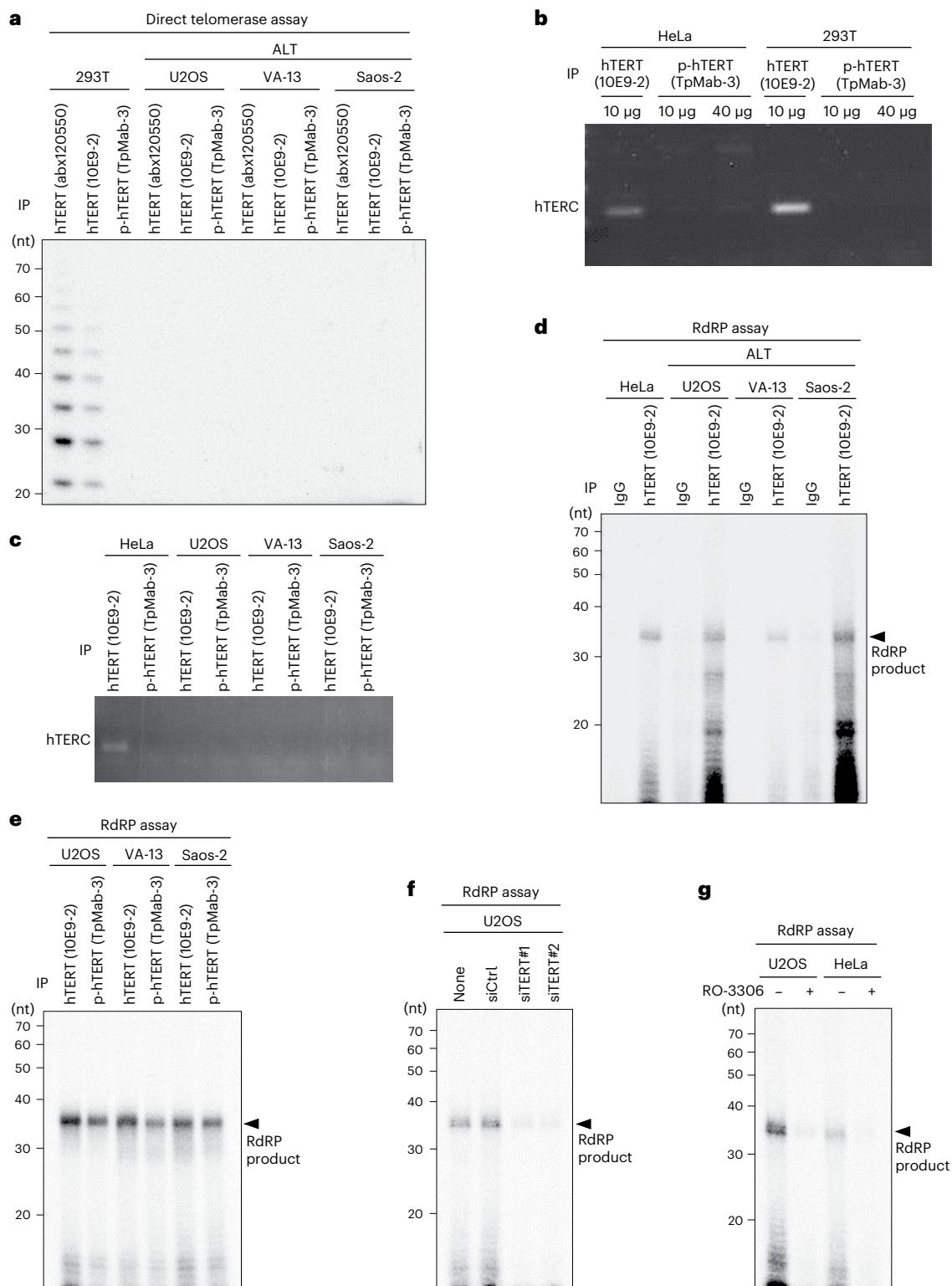


Fig. 2 | Enzymatic activity of hTERT in ALT cells. a, Telomerase activity of hTERT and p-hTERT immunoprecipitated with anti-hTERT (abx120550 and 10E9-2) and anti-p-hTERT (TpMab-3) antibodies from the indicated cells. The 293T cells are positive controls. **b, c**, Association of hTERC with hTERT and p-hTERT isolated with the 10E9-2 and the TpMab-3 antibodies from HeLa, 293T (**b**) and ALT cells (U2OS, VA-13, and Saos-2 cells; **c**). **d**, IP-RdRP assay using hTERT protein prepared

identically to those in **a** from cells treated with nocodazole. Mouse IgG is an isotype control for the immunoprecipitation. **e**, IP-RdRP assay using hTERT and p-hTERT proteins from cells treated with nocodazole. **f, g**, RdRP activity of mitotic U2OS cells with hTERT knockdown (**f**) or CDK1 inhibition (RO-3306; **g**). Experiments were repeated three times with similar results. Source unprocessed blots are available as source data.

examined whether the AS variants of hTERT exhibit RdRP activity using recombinant hTERT AS variant proteins. Although we detected α , β , γ and Δ 4-13 variants as well as the full-length hTERT mRNA in U2OS cells

(Extended Data Fig. 3a,b), recombinant AS variant proteins exhibited no RdRP activity (Extended Data Fig. 3c,d). These results indicate that the full-length hTERT is essential for the RdRP activity.

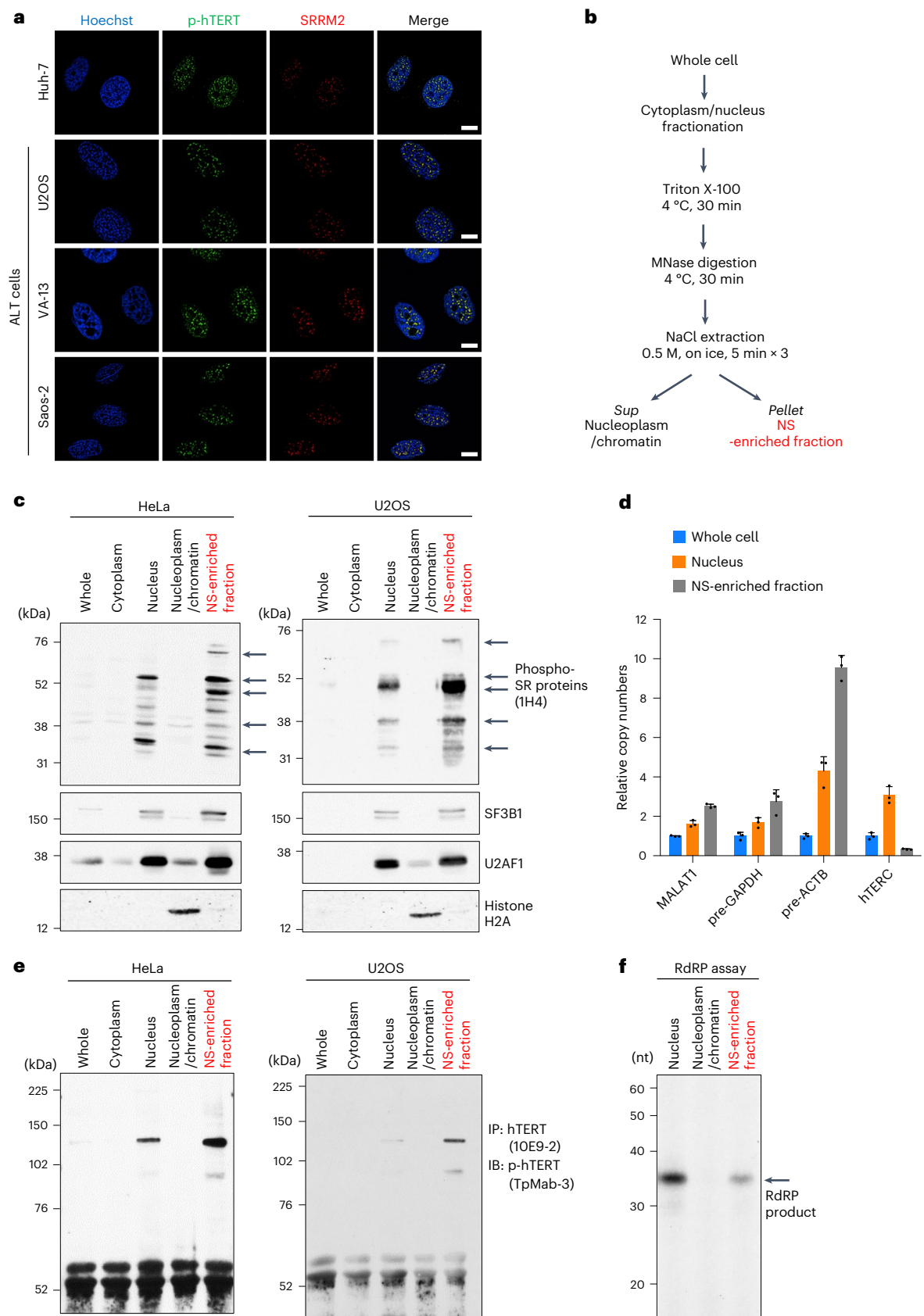


Fig. 3 p-hTERT localizes in NSs in ALT cells. **a**, Super-resolution imaging of p-hTERT and SRRM2 in Huh-7, U2OS, VA-13 and Saos-2 cells. Scale bars, 10 μ m. **b**, Strategy for biochemical purification of NS-enriched fraction. **c**, Detection of NS marker proteins such as phospho-SR proteins (clone 1H4), SF3B1 and U2AF1 in the NS-enriched fraction. H2A is a marker for chromatin proteins. **d**, Determination of hTERC levels in NSs by quantitative RT-PCR analysis. MALAT1 long noncoding RNA

and precursor mRNAs (pre-GAPDH and pre-ACTB) are marker RNAs localized in NSs. Data are presented as mean \pm s.d. ($n = 3$ independent experiments per group). **e**, Detection of hTERT proteins immunoprecipitated from the indicated biochemical fractions. **f**, IP-RdRP assay using hTERT proteins prepared identically to those in **e**. Experiments were repeated four times (**e**), three times (**c, f**), and twice (**a**) with similar results. Numerical source data and unprocessed blots are available as source data.

p-hTERT localizes in nuclear speckles in ALT cells

To study a functional role of p-hTERT in ALT cells, we initially examined localization of p-hTERT in ALT cells. The hTERT signal, which includes both unphosphorylated and phosphorylated hTERT, exists throughout the nucleus, whereas p-hTERT localizes in the nuclear structures (Extended Data Fig. 4a). The formation of ALT-associated promyelocytic leukaemia (PML) bodies (APBs) around telomeres is essential for the maintenance of telomeres in ALT cells²⁹. However, the signal of p-hTERT did not colocalize with that of APB markers PML and TRF2 in U2OS cells (Extended Data Fig. 4b,c), indicating that p-hTERT exists outside telomeres. We focused on the shape of p-hTERT signals in immunofluorescence imaging. Emerging evidence has shown that RNA and intrinsically disordered proteins undergo liquid–liquid phase separation (LLPS) to form liquid droplets inside the cells^{30,31}. Since p-hTERT forms foci like liquid droplets (Fig. 1a and Extended Data Fig. 4a), we hypothesized that p-hTERT undergoes LLPS and subsequently localizes in subnuclear structures. Proteins, potentially inducing LLPS, harbour intrinsically disordered regions (IDRs) on their protein domains³². Putative analyses of IDRs by several web interfaces predicted the existence of an IDR on hTERT protein (Extended Data Fig. 4d–g). To confirm the involvement of LLPS, we treated HeLa and U2OS cells with 1,6-hexanediol (1,6-HD) which disrupts hydrophobic interactions and inhibits LLPS. Treatment with 1,6-HD rapidly disassembled the dot structure of p-hTERT (Extended Data Fig. 4h), suggesting that p-hTERT localizes in subnuclear structures formed by LLPS. The 1,6-HD treatment also allowed us to efficiently detect endogenous hTERT (Extended Data Fig. 4i) and its RdRP activity (Extended Data Fig. 4j). In addition, we lysed cells in high salt to inhibit weak electrostatic interactions, since the electrostatic interactions are essential for LLPS. Each treatment with 1 M NaCl and 1,6-HD increased the hTERT protein amounts isolated from U2OS and HeLa cells (Extended Data Fig. 4k). Combination of treatments with 1 M NaCl and 1,6-HD further enriched the yield of hTERT proteins recovery (Extended Data Fig. 4k). These observations suggest that p-hTERT does not co-localize with telomeres but is present in another subnuclear structure through LLPS in both telomerase-positive and ALT cells.

Next, we assessed where p-hTERT is localized. We focused on NSs that contain RNA regulators such as precursor mRNA (pre-mRNA) splicing factors, transcription factors and 3'-end RNA processing factors^{33,34}, because p-hTERT regulates the expression of specific genes by synthesizing antisense RNAs^{15,16}. Multicolour immunofluorescence imaging using a super-resolution microscopy demonstrated that the signal of p-hTERT completely merged with an NS marker SRRM2 in ALT cells (Fig. 3a). We then confirmed that the p-hTERT antibody (TpMab-3) does not cross-react to phospho-Ser-Arg-rich (SR) proteins contained abundantly in NSs. While the treatment with hTERT siRNAs eliminated the p-hTERT signal, it did not affect the signal of phospho-SR proteins (Extended Data Fig. 5a). Furthermore, we treated cells with a CLK1 inhibitor KH-CB19 to inhibit phosphorylation of SR proteins, because CLK1 is a specific kinase for SR proteins³⁵. The treatment with the CLK1 inhibitor inhibited the phosphorylation of SR proteins, but not that of hTERT (Extended Data Fig. 5b).

To further confirm the localization of p-hTERT in NSs, we biochemically isolated an NS-enriched fraction (Fig. 3b and Methods). We confirmed that the NS-enriched fraction contained a series of

phospho-SR proteins, SF3B1, and U2AF1 that are marker proteins localized in NSs (Fig. 3c). We also observed the enrichment of pre-mRNAs and MALAT1 long noncoding RNA in the NS-enriched fraction, which were localized in NSs³⁶. By contrast, we found that hTERT is less abundant in the NS-enriched fraction than in nuclear fraction (Fig. 3d). IP-IB assay using an anti-p-hTERT antibody demonstrated that this purification process concentrated p-hTERT into the NS-enriched fraction (Fig. 3e). In addition, hTERT immunoprecipitated from the NS-enriched fraction exhibited RdRP activity (Fig. 3f). These results indicate that p-hTERT localizes outside telomeres but in NSs in both telomerase-positive and ALT cells.

RdRP regulates R-loop structure on TERRA sequences

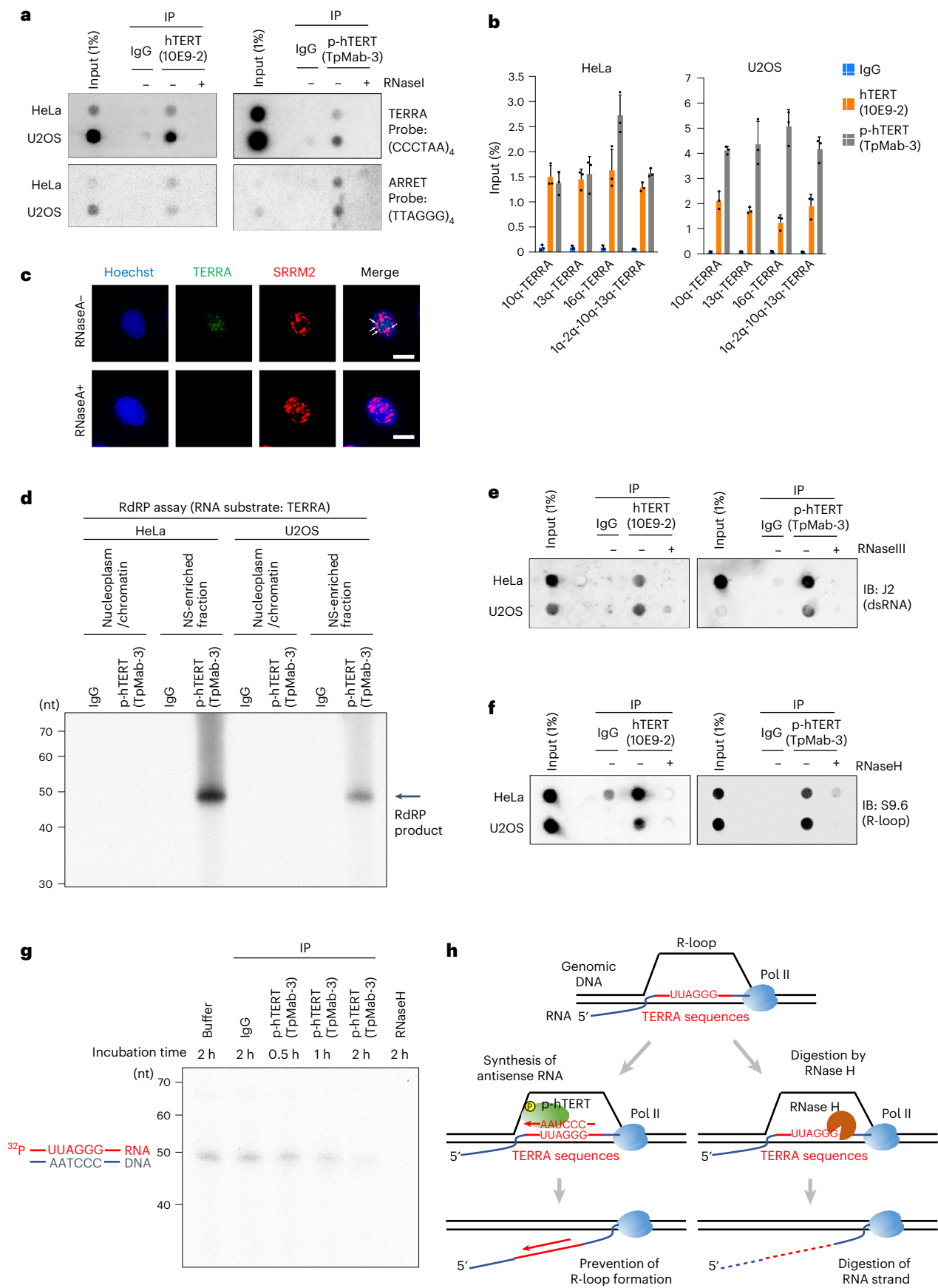
To investigate the function of p-hTERT in NSs, we isolated hTERT complex by IP from NSs purified biochemically and conducted RIP-seq analysis for RNAs associated with hTERT in NSs (Extended Data Fig. 6a). Interestingly, the RIP-seq suggested that hTERT interacts with TERRA RNAs³⁷ transcribed from subtelomeric regions (Extended Data Fig. 6b). We also verified the association of hTERT and p-hTERT with TERRA RNAs by RNA dot blot analysis (Fig. 4a) and qRT-PCR analysis (Fig. 4b). hTERT knockdown cells had higher levels of TERRA RNA expression (Extended Data Fig. 6c). Since we studied the NS fraction in these analyses, these results suggest that TERRA RNAs exist in NSs. In concordance with these findings, previous reports revealed that not all TERRA RNAs localize at telomeres and some TERRA RNAs exist outside telomeres, although TERRA RNAs are enriched at telomeres^{38,39}. To further investigate the localization of TERRA RNAs into NSs, we performed FISH (fluorescence in situ hybridization) analyses for TERRA RNAs and verified that TERRA RNAs localized in NSs (Fig. 4c).

To examine whether p-hTERT exhibits RdRP activity with TERRA RNAs, we used TERRA RNAs as a template for IP-RdRP assay and confirmed that hTERT (Extended Data Fig. 6d) and p-hTERT (Fig. 4d) synthesized RdRP products using TERRA RNAs as a template. To determine whether TERRA RNAs are preferentially used for RdRP activity, we performed a titration assay using a mixture of template TERRA RNAs and artificial RNAs without TERRA sequences and found that TERRA RNAs exhibited robust RdRP activity (Extended Data Fig. 6e). Moreover, hTERT and p-hTERT purified from NSs interact with double-stranded RNAs (dsRNAs) detected with a dsRNA-specific antibody (Fig. 4e). These observations revealed that hTERT RdRP synthesizes antisense RNAs of TERRA RNAs and produces dsRNAs. Since TERRA RNAs have been shown to associate with telomeric repeat sequences in genomic DNA and form RNA–DNA hybrid (R-loop) structures^{38,40}, we speculated that hTERT might also regulate R-loop formation especially on TERRA sequences. An analysis of hTERT and p-hTERT immunoprecipitated from NSs identified R-loop signals associated with hTERT and p-hTERT (Fig. 4f). To clarify a function of p-hTERT in R-loop regulation, we incubated telomeric repeat RNA–DNA hybrids with hTERT (Extended Data Fig. 6f,g) and p-hTERT (Fig. 4g) immune complex and observed degradation of telomeric repeat RNA–DNA hybrids, suggesting that p-hTERT dissolves R-loop structures. We obtained these data using hTERT and p-hTERT purified from NSs fractions, indicating that the R-loop regulation by RdRP occurs in NSs. Given these results, we propose a model for regulation of R-loop formation via RdRP reaction (Fig. 4h). Following RNA transcription, nascent RNA transcript and DNA template hybridize

Fig. 4 | Involvement of RdRP in R-loop resolution on TERRA sequences.

a,b, Detection of TERRA and ARRET RNAs associated with p-hTERT immunoprecipitated from NS-enriched fraction, analysed by RNA dot blot (**a**) and quantitative RT-PCR analyses (**b**; $n = 3$ independent experiments per group). Data are presented as mean \pm s.d. **c**, FISH for TERRA RNAs in U2OS cells. An NS marker SRRM2 is co-stained. Treatment with RNase A was included as a control. Scale bars, 10 μ m. **d**, RdRP activity of p-hTERT purified from NSs against a synthetic TERRA RNA template. **e,f**, Dot blot analyses of dsRNAs (**e**) and R-loop structures (**f**) using RNAs and gDNAs associated with p-hTERT in NSs.

Treatment with dsRNA-specific RNase III and RNA–DNA hybrid-specific RNase H was included as controls. **g**, In vitro R-loop degradation assay using p-hTERT complex immunoprecipitated from the NS-enriched fraction and 5'-³²P-labelled TERRA RNA–DNA hybrids. The reaction products were treated with RNase III to remove dsRNAs generated by RdRP activity of p-hTERT. RNase H is a positive control to digest RNA–DNA hybrids. **h**, Model of resolution of R-loop structures by p-hTERT. Experiments were repeated three times (**a,e,f**) and twice (**c,d,g**) with similar results. Numerical source data and unprocessed blots are available as source data.



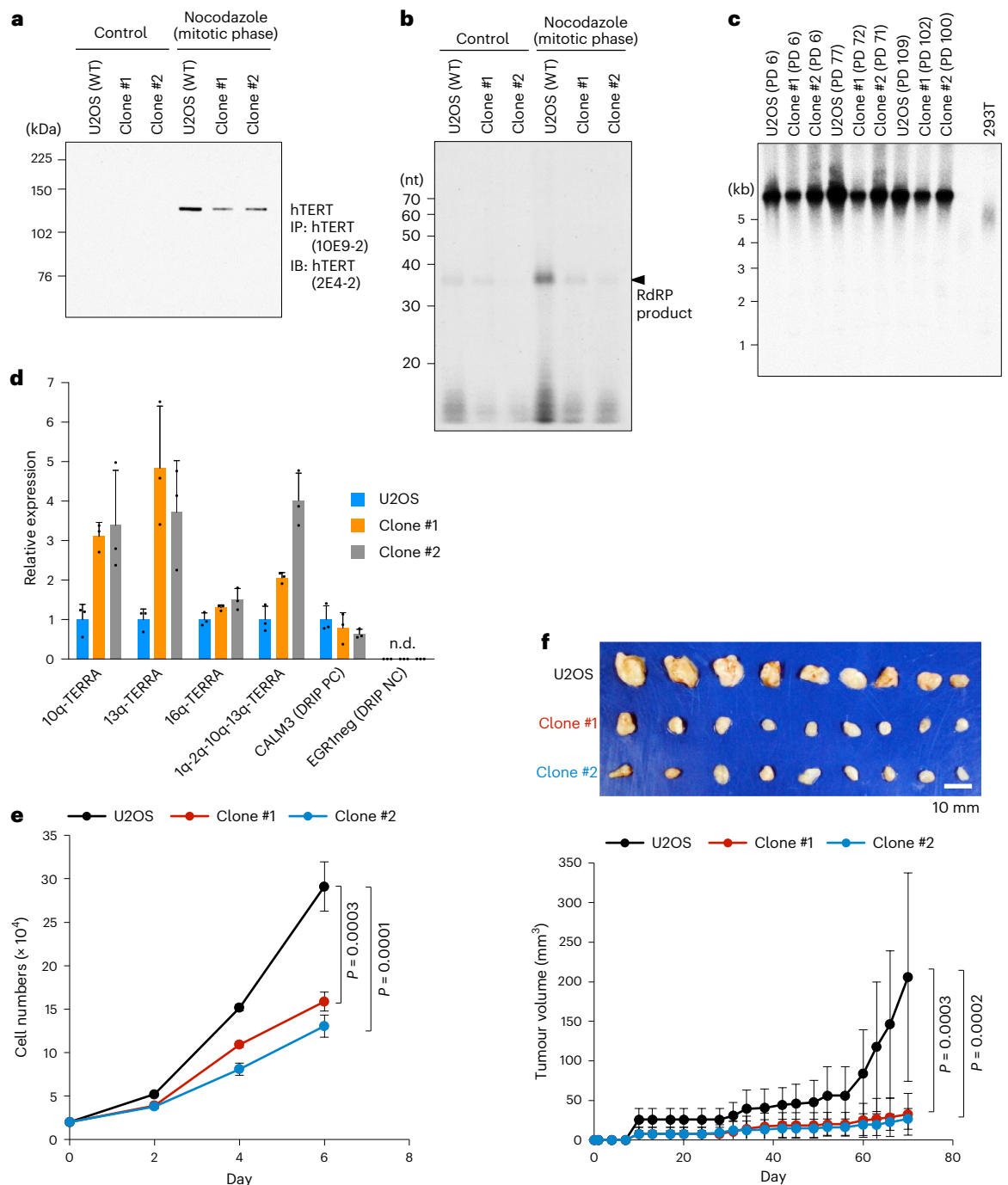


Fig. 5 | CRISPR-Cas9 editing of *TERT* gene locus in U2OS cells. a, Expression of hTERT protein (2E4-2) in hTERT-CRISPR clones with nocodazole treatment. **b**, IP-RdRP assay using hTERT-CRISPR clones treated as in **a**. **c**, Evaluation of telomere lengths in hTERT-CRISPR clones by Southern blotting analysis for telomere restriction fragments. PD, population doublings. **d**, Determination of TERRA RNA levels by quantitative RT-PCR analysis of DRIP products. CALM3 and ERG1 were analysed as positive and negative controls, respectively, for DRIP analysis. n.d., not detected. Data are presented as mean \pm s.d. ($n = 3$ independent experiments

per group). **e**, Cell proliferation assay using hTERT-CRISPR clones. Data are presented as mean \pm s.d. ($n = 3$ independent experiments per group). **f**, Tumours generated from hTERT-CRISPR clones in NOD/SCID mice (top panel). The volume of each tumour is shown as mean \pm s.e.m. ($n = 8$ mice per group; bottom panel). One-way ANOVA with Dunnett correction for multiple comparisons between control and other groups (**e**, **f**). Experiments were repeated three times (**a**, **b**) or twice (**c**) with similar results. Numerical source data and unprocessed blots are available as source data.

and form R-loop structures, where p-hTERT binds to TERRA sequences of the nascent RNA transcripts and synthesizes antisense RNAs through RdRP activity. The RdRP reaction converts RNA–DNA hybrids of R-loops to dsRNAs, preventing R-loop formation. Since an accumulation of R-loop formation has anti-proliferative effects, by resolving R-loops hTERT may allow the proliferation of ALT cells.

TERT gene editing impairs the proliferation of ALT cells

To further assess the biological significances of p-hTERT in ALT cells, we used the CRISPR-Cas9 system targeting the *TERT* gene. We failed to develop hTERT knockout clones with homozygous mutations, probably because the loss of *TERT* gene is lethal. However, we established two clones with heterozygous mutations in the *TERT* gene. We found by

Sanger sequencing analysis that hTERT-CRISPR clone #1 has an allele with 16 bp deletion (853–868 nt in exon 2) in the *TERT* locus in addition to wild-type allele (Extended Data Fig. 7a), and that hTERT-CRISPR clone #2 has two mutant alleles with 16 bp deletion (848–863 nt or 853–868 nt in exon 2) in the *TERT* locus (Extended Data Fig. 7b). These 16 bp deletion mutations result in frameshifting and causes a premature termination codon (PTC; 1,033 nt from the transcription start site). The PTC in the coding region of hTERT mRNA would be recognized and degraded by nonsense-mediated mRNA decay⁴¹. Indeed, hTERT expression both in hTERT-CRISPR clones #1 and #2 was lower than that in wild-type U2OS cells at protein (Fig. 5a) and mRNA (Extended Data Fig. 7c) levels. Furthermore, we observed that CRISPR-Cas9 editing of the *TERT* locus ablated the RdRP activity dependent on hTERT (Fig. 5b). Genome edition of the *TERT* gene did not affect telomere lengths in U2OS cells, confirming that hTERT is not involved in telomere maintenance in ALT cells (Fig. 5c). To investigate R-loop structures in hTERT-CRISPR clones, we performed DRIP (DNA–RNA immunoprecipitation) assay with an RNA–DNA hybrid-specific S9.6 antibody and determined TERRA RNA levels contained in R-loop structures. This analysis demonstrated that TERRA RNAs are more abundant in DRIP samples of hTERT-CRISPR clones than those of wild-type U2OS cells, suggesting that R-loops with TERRA RNAs accumulate in hTERT-CRISPR clones (Fig. 5d). We next performed RNA-seq and clustering of expression profiles on the subset of genes expressed differentially in hTERT-CRISPR clones. The subsequent gene ontology (GO) analysis showed enrichment of genes involved in cell cycle process and DNA replication within genes down-regulated in hTERT-CRISPR clones (Extended Data Fig. 7d). We then monitored the proliferation of these cells. The *TERT* gene mutation in hTERT-CRISPR clones #1 and #2 negatively affected cell proliferation (Fig. 5e). To further evaluate the influence of *TERT* gene editing in ALT cells in vivo, we implanted wild-type U2OS cell and hTERT-CRISPR clones (clone #1 and #2) subcutaneously into non-obese diabetic/severe combined immunodeficiency (NOD/SCID) mice. Consistent with the results of the cell proliferation assay, the volume of tumours generated using hTERT-CRISPR clones (clone #1 and #2) was significantly smaller than that of wild-type U2OS control (Fig. 5f).

Synthetic lethality between inhibition of RdRP and FANC/BRCA

Next, we performed genome-wide CRISPR screening using cell lines that harbour the mutant hTERT-CRISPR allele. We infected the hTERT-CRISPR clone with the Brunello human CRISPR/Cas9 lentiviral library⁴², which contains 76,441 single-guide RNAs (sgRNAs) targeting 19,114 genes. After puromycin selection, we collected a portion of the cells as a sample for day 0, and we then collected the rest of cells after 21 days of culture (Fig. 6a). We conducted next-generation sequencing to determine sgRNAs contained in each cell population and plotted the gene essentiality score calculated with the MAGeCK algorithm⁴³ (Fig. 6b). We focused on gene groups with lower essentiality scores (< -0.5) for the hTERT-CRISPR clone but not for wild-type U2OS cells, implying that these genes are specifically essential for the hTERT-CRISPR clone (Fig. 6b). The subsequent GO analysis and pathway

analysis of these genes showed the enrichment of genes involved in DNA repair and Fanconi anaemia (FANC) pathway (Fig. 6c,d). These genes included *BRCA1*, *BRCA2* and FANC genes (Fig. 6e), which function in DNA repair processes in concert with *BRCA1* and *BRCA2*^{44,45}. Deletion of the FANC/BRCA genes only exhibited an effect in the absence of hTERT expression (Fig. 6e). To assess synthetic lethality by inhibition of hTERT and the FANC/BRCA pathway, we induced knockdown of genes involved in the FANC/BRCA pathway in hTERT-CRISPR clones (Extended Data Fig. 8a). Suppression of FANC/BRCA gene expression with these siRNAs significantly decreased the viability of hTERT-CRISPR clones more greatly than that of U2OS cells (Fig. 6f and Extended Data Fig. 8b). The CRISPR screening did not define *PARP1* as an essential gene for the hTERT-CRISPR clone (Extended Data Fig. 8c), although *PARP1* also plays an important role in DNA repair⁴⁶. Indeed, *PARP1* knockdown did not have an effect on the viability of hTERT-CRISPR clones (Extended Data Fig. 8d,e). We then overexpressed wild-type or T249A-mutant hTERT in hTERT-CRISPR clones to validate the significance of RdRP activity in the synthetic lethality (Extended Data Fig. 8f). T249A-mutant, in which the threonine 249 of hTERT is replaced with alanine, is not phosphorylated and thus lacks the RdRP activity¹⁶. Although overexpression of wild-type hTERT rescued the synthetic lethal phenotype of hTERT-CRISPR clones with FANC/BRCA knockdown, overexpression of the T249A-mutant had no effect on the viability of hTERT-CRISPR clones (Fig. 6g and Extended Data Fig. 8g). These results suggest that the RdRP activity, but not other functions, is involved in the synthetic lethal pathway.

Next, we induced hTERT knockdown in telomerase-positive Capan-1 cells (Extended Data Fig. 9a,b), which carry a *BRCA2* mutation, and Capan-1 clones reverted from *BRCA2* mutation, in which *BRCA2* gene expression is restored⁴⁷. The Capan-1 clones with reversion of *BRCA2* gene mutation exhibited a significantly higher survival rate after treatment with siTERT #1 and #2 than that in control Capan-1 cells (Fig. 6h and Extended Data Fig. 9c). We also utilized FANCF-deficient TOV-21G cells and TOV-21G cells corrected for FANCF (designated TOV-21G FANCF)⁴⁸. TOV-21G FANCF cells were more resistant to hTERT knockdown (Fig. 6i and Extended Data Fig. 9d) and to a CDK1 inhibitor RO-3306, which blocks the RdRP activity, as well as to a *PARP1* inhibitor, olaparib, used as a positive control (Fig. 6j,k and Extended Data Fig. 9e,f). By contrast, when we treated these cells with a telomerase inhibitor, 6-thio-dG⁴⁹, both TOV-21G and TOV-21G FANCF cells were not resistant to the telomerase inhibitor (Fig. 6l and Extended Data Fig. 9g), implying that inhibition of telomerase activity did not induce the synthetic lethality. Collectively, these observations reveal that inhibition of RdRP and the FANC/BRCA pathway is synthetic lethal.

Inhibition of RdRP and FANC/BRCA accumulates R-loops

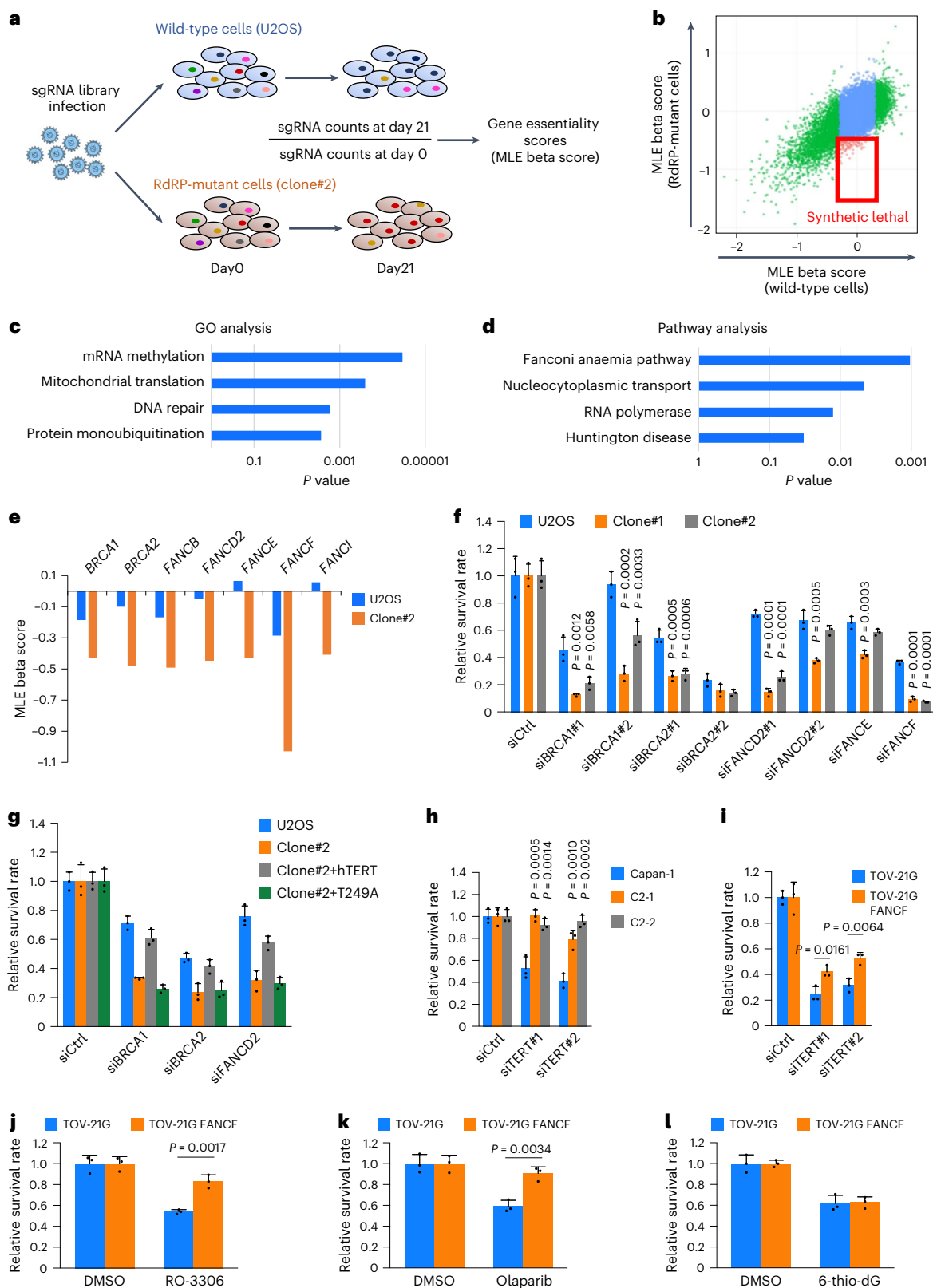
Biochemical experiments demonstrated that p-hTERT regulates a formation of R-loop structures (Fig. 4). Notably, previous reports have also shown that FANC/BRCA genes, including *BRCA1*, *BRCA2* and *FANCD2*, dissolve R-loop structures and prevent excessive R-loop accumulation^{50–52}. To investigate cooperative control in R-loop formation by hTERT and FANC/BRCA pathway, we induced double-knockdown of hTERT and FANC/BRCA gene and analysed R-loop levels in the cells.

Fig. 6 | Synthetic lethality between inhibition of RdRP and Fanconi anaemia/BRCA. **a**, Scheme of genome-wide CRISPR screening using an RdRP-mutant hTERT-CRISPR clone. U2OS cells and hTERT-CRISPR clone #2 were transduced with lentivirus gRNA library and selected with puromycin for 48 h, and a portion of the cells was collected as a baseline (day 0). The remainder was harvested after 21 days of culture. **b**, The MLE beta scores for each gene generated using the MAGeCK algorithm, which shows gene essentiality in the cells. The red square indicates RdRP synthetic lethal genes. **c,d**, GO analysis (**c**) and KEGG pathway analysis (**d**) for RdRP synthetic lethal genes. The *P* values were calculated using the clusterProfiler package. **e**, The MLE beta essentiality scores for FANC/BRCA genes. **f**, Colony formation assay using hTERT-CRISPR clones transfected with siRNAs specific for FANC/BRCA genes ($n = 3$ independent experiments

per group). **g**, Survival of hTERT-CRISPR clones with FANC/BRCA knockdown when overexpressing a wild-type hTERT or an RdRP-deficient T249A mutant ($n = 3$ independent experiments per group). **h,i**, Survival rates following hTERT knockdown in Capan-1 (**h**) and TOV-21G (**i**) cell clones corrected for *BRCA2* and FANCF deficiencies, respectively ($n = 3$ independent experiments per group). **j–l**, Sensitivity of TOV-21G FANCF cells to a CDK1 inhibitor (RO-3306; **j**), a *PARP1* inhibitor (olaparib; **k**) and a telomerase inhibitor (6-thio-dG; **l**) ($n = 3$ independent experiments per group). Data are presented as mean \pm s.d. (**f–l**). Two-tailed unpaired *t*-test (**i–k**) and one-way ANOVA method with Dunnett correction for multiple comparisons between control and other groups (**f,h**). Numerical source data are available as source data.

R-loop signals accumulated after single-knockdown of hTERT (Fig. 7a, leftmost lane). In addition, slight accumulation of R-loop signals was observed in single-knockdown of FANC/BRCA genes (Fig. 7a, right four lanes, first line). Strikingly, they were particularly enriched in the cells with double-knockdown of hTERT and FANC/BRCA genes (Fig. 7a, right four lanes, second and third lines). In addition, we immunoprecipitated R-loop structures from the cells by DRIP⁵³ and determined

TERRA RNA levels associated with R-loops by a strand-specific reverse transcription and the subsequent qPCR (Extended Data Fig. 9h,i). Consistent with the dot blot analysis, this DRIP analysis found that TERRA RNAs associated with R-loop structures accumulated in the cells with double-knockdown of hTERT and FANC/BRCA genes (Fig. 7b). These observations demonstrated that inhibition of hTERT and the FANC/BRCA pathway leads to accumulation of R-loop structures. We were



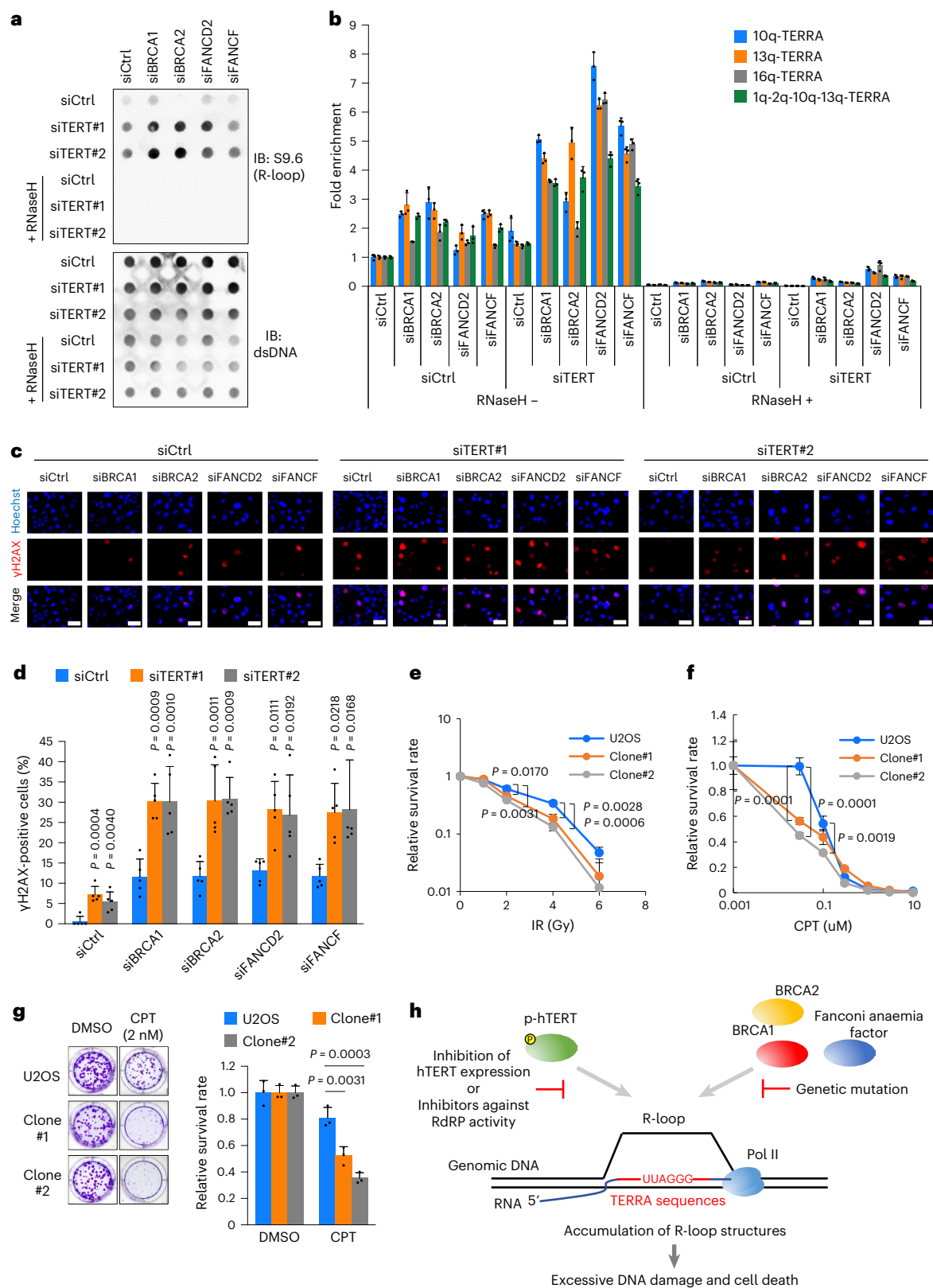


Fig. 7 | Genome instability triggered by suppression of hTERT. a, b, Analyses of R-loop structures in U2OS cells co-transfected with siRNAs specific for hTERT and FANCF/BRCA genes. R-loop structures were detected by dot blot analysis (a). TERRA RNA levels in R-loops were determined by strand-specific quantitative RT-PCR analysis of DRIP products ($n = 3$ independent experiments per group). RNase H, a control to digest RNA–DNA hybrids; dsDNA, a loading control. **c, d,** IIF imaging of γ H2AX in U2OS cells with double-knockdown of hTERT and FANCF/BRCA genes ($n = 4$ independent experiments per group). Scale bars, 50 μ m.

e–g, Cell viability assays using hTERT-CRISPR clones treated with IR (e) and CPT (f; $n = 3$ independent experiments per group). Cell viability was determined by colony formation assay (e, g) and MTT assay (f). **h,** Model of synthetic lethality between inhibition of RdRP activity and the FANCF/BRCA pathway. Data are presented as mean \pm s.d. (b, d–g). One-way ANOVA with Dunnett correction for multiple comparisons between control and other groups (d–g). Experiments were repeated three times (a) or twice (c) with similar results. Numerical source data and unprocessed blots are available as source data.

unable to detect interaction of RdRP with BRCA2, suggesting that RdRP and the FANC/BRCA pathway function redundantly (Extended Data Fig. 10a,b). Excessive R-loop structures cause DNA damage and subsequent genome instability². Consistently, double-knockdown of hTERT and FANC/BRCA genes efficiently induced γ H2AX, which is a marker associated with DNA lesions (Fig. 7c,d). Therefore, we finally examined the effect of hTERT on vulnerability to DNA damage. In results, hTERT-CRISPR clones were more sensitive to DNA damage induced by ionizing radiation (IR) and camptothecin (CPT; Fig. 7e–g). Taken together, hTERT RdRP dissolves R-loop structures on TERRA sequences and guarantees genomic stability, like the FANC/BRCA proteins (Fig. 7h and Extended Data Fig. 10b).

Discussion

Expression and activity of p-hTERT in ALT cells

The discovery of ALT activity in immortalized cell lines without telomerase activity was first reported in 1995. The authors revealed that these ALT cells completely lack telomerase activity²³ and that the ALT mechanism occurs in human tumours²⁴. The subsequent studies have shown that most cancer cells with ALT activity lack telomerase activity and maintain the telomere without any contribution of hTERT^{23,24,54–56}. This series of studies resulted in emphasizing the mutually exclusive properties of telomerase and ALT activities, and hence, the expression of hTERT in ALT cells has scarcely been investigated. However, several reports verified that hTERT is functional in ALT cells^{54–56}. For example, ectopic expression of a mutant hTERT in ALT cells showed that hTERT contributes to tumorigenesis by a telomerase-independent manner in ALT cells²⁵. In this study, we have focused on the role of hTERT in ALT cells lacking telomerase activity (Figs. 1 and 3) and provided evidence showing that p-hTERT exhibits RdRP activity but not telomerase activity (Fig. 2). Genome editing of the *TERT* gene in ALT cells had inhibitory effects on proliferation of ALT cells (Fig. 5). These observations reveal that p-hTERT in ALT cells exhibits RdRP activity and contributes to cancer progression in a telomerase-independent manner. We previously conducted genome editing of *TERT* in telomerase-positive 293T cells and demonstrated that the genome editing of *TERT* in 293T cells also inhibited tumour formation¹⁶. Taken together, these results suggest that the RdRP activity of hTERT contributes to cancer progression in various cells including telomerase-positive and ALT cells.

One question is why ALT cells do not show telomerase activity. We confirmed expression of both minimum essential components for telomerase activity, hTERT and hTERC, in ALT cells (Fig. 1). Despite the expression of hTERT and hTERC, ALT cells did not exhibit telomerase activity (Fig. 2a). We noticed that the signal of p-hTERT completely merged to NS markers, indicating that p-hTERT mostly, if not completely, localizes in NSs of ALT cells (Fig. 3a). Furthermore, we observed rare hTERC signal in NSs (Fig. 3d), probably because hTERC localizes partly in another subnuclear structure, Cajal body, with hTERT, which is essential for the maturation of telomerase enzyme complex⁵⁷. These results imply that p-hTERT and hTERC exist in separate compartments. We previously reported that phosphorylation of hTERT promotes RdRP activity but dispensable for telomerase activity¹⁶. In addition, we confirmed that p-hTERT does not exhibit telomerase activity even in telomerase-positive 293T cells (Fig. 2a), and that p-hTERT does not associate with hTERC, even if hTERC is present (Fig. 2b). We also found that hTERT does not form a complex with hTERC in ALT cells (Fig. 2c). Alternatively, hTERT binds to TERRA RNAs in ALT cells (Fig. 4a,b). Previous reports demonstrated that ALT cells express high levels of TERRA RNAs^{38,58} and that TERRA RNAs associate with hTERC and inhibit telomerase activity³⁹. These data suggest that TERRA RNAs might inhibit the formation of telomerase complex in ALT cells.

Detection of endogenous hTERT proteins

While we detected hTERT proteins in mitotic cells, hTERT was difficult to detect in cells without nocodazole treatment (Fig. 1g,h). Consistent

with our data, several groups have reported that it is difficult to detect endogenous hTERT in interphase^{59,60} and that hTERT is enriched in mitotic phase⁶¹. In the present study, we revealed that endogenous hTERT localizes in NSs in interphase (Fig. 3a), and found that treatment to disassemble the NS structure with 1,6-HD promotes to solubilize hTERT proteins even in interphase (Extended Data Fig. 4i). We consider that the manipulation of cells in mitosis, where nuclear membrane disappears and nuclear structures disassemble, is equivalent to the treatment with 1,6-HD (Fig. 1f). These results suggest that the disassembly of NS structures would enable us to solubilize and efficiently detect hTERT proteins.

Regulation of R-loop formation by p-hTERT

In terms of the physiological significance of hTERT, we demonstrate that hTERT regulates R-loop structure through RdRP (Fig. 4). To prevent the deleterious effects of accumulation of R-loop structures, cells express regulators of R-loop structures, including RNase H family protein^{3,4} and helicases such as SETX⁵ and DHX9⁶. A previous ChIP-seq analysis revealed the predominant association of RNase H1 with R-loops in gene promoter regions⁶². Since it is not clear in this previous study whether RNase H1 regulates TERRA RNAs, we analysed their ChIP-seq data and found no binding signal of RNase H1 in subtelomeric regions. In the present study, we report that hTERT associates with and dissolves R-loop structures on TERRA sequences (Fig. 4), suggesting that hTERT regulates R-loop structures by different mode of action from RNase H1.

We propose a model for regulation of R-loop formation via RdRP reaction (Fig. 4h). In this model, the RdRP reaction targeting TERRA sequences strips RNA transcripts from the RNA–DNA hybrids to dissolve R-loop structures. Consistent with our model, a previous report indicated that R-loop formation in transcription termination regions facilitates synthesis of antisense RNAs that hybridize with the sense RNAs, subsequently generating dsRNAs⁶³. Although this previous report did not provide any data on what kind of polymerases catalyse the synthesis of antisense RNAs, we here discovered that p-hTERT is a synthesizer of antisense RNAs in genomic regions with R-loops. Our data support and strengthen the model that generation of dsRNAs through synthesizing antisense RNAs regulates R-loop formation.

Gene dependency of ALT cells

A previous report analysed the gene dependency of ALT cells, indicating that ALT cells depend on genes involved in DNA replication and replication stress response⁶⁴. In particular, this analysis demonstrated that *FANCM* is the most essential gene in ALT cells, probably because FANCM suppresses telomeric replication stress in ALT cells⁶⁵. Consistent with this previous finding, the CRISPR screening in this study identified *FANCM* as a gene with high dependency in wild-type U2OS cells, and revealed that *FANCM* was also essential for hTERT-CRISPR clones. These observations imply that *FANCM* is an essential gene in ALT cells, regardless of hTERT status.

Inhibition of RdRP activity and FANC/BRCA pathway

Several laboratories have reported that the FANC/BRCA family members remove R-loop structures, thereby preventing genome instability^{50–52}. In particular, association of BRCA1 with TERRA RNAs prevented the formation of R-loops mediated by TERRA RNAs⁵². In the current study, we performed a genome-wide CRISPR/Cas9 loss of function screen and revealed that concurrent inhibition of hTERT and the FANC/BRCA genes significantly decreased cell viability (Fig. 6). hTERT did not associate with BRCA2, suggesting that RdRP and FANC/BRCA pathway function redundantly (Extended Data Fig. 10). The FANC/BRCA genes maintain genomic DNA homeostasis, suppressing cancer progression, and cells lacking the FANC/BRCA pathway are more cancer prone⁶⁶. Therefore, inhibition of the RdRP activity of hTERT may be an effective therapeutic strategy for such tumours lacking the FANC/BRCA pathway.

In summary, our results indicate that p-hTERT is universally expressed in not only telomerase-positive cells but also ALT cells. We further found the localization of p-hTERT into NSs and affirmed that p-hTERT regulates R-loop formation through RdRP activity, which contributes to cancer cell proliferation. These observations implicate that p-hTERT maintains genome stability throughout the genome from telomere to telomere by taking advantage of the two distinct enzymatic activities (Extended Data Fig. 10c). These results provide important insights for a deeper understanding of the mechanisms underlying the telomerase-independent contribution of hTERT to tumours.

Inclusion and ethics statement

All collaborators of this study have fulfilled all authorship criteria required by Nature Portfolio journals and have been listed as authors, as their participation was essential for this study throughout the research process. Findings in this study were determined with these local collaborators. The collaborators agreed on their roles and responsibilities ahead of the research. This research was not severely restricted or prohibited in the setting of the researchers. This research does not result in stigmatization, incrimination, discrimination or otherwise personal risk to participants.

Online content

Any methods, additional references, Nature Portfolio reporting summaries, source data, extended data, supplementary information, acknowledgements, peer review information; details of author contributions and competing interests; and statements of data and code availability are available at <https://doi.org/10.1038/s41556-024-01427-6>.

References

- Roos, W. P., Thomas, A. D. & Kaina, B. DNA damage and the balance between survival and death in cancer biology. *Nat. Rev. Cancer* **16**, 20–33 (2016).
- Petermann, E., Lan, L. & Zou, L. Sources, resolution and physiological relevance of R-loops and RNA-DNA hybrids. *Nat. Rev. Mol. Cell Biol.* **23**, 521–540 (2022).
- Nowotny, M. et al. Structure of human RNase H1 complexed with an RNA/DNA hybrid: insight into HIV reverse transcription. *Mol. Cell* **28**, 264–276 (2007).
- Rychlik, M. P. et al. Crystal structures of RNase H2 in complex with nucleic acid reveal the mechanism of RNA-DNA junction recognition and cleavage. *Mol. Cell* **40**, 658–670 (2010).
- Skourti-Stathaki, K., Proudfoot, N. J. & Gromak, N. Human senataxin resolves RNA/DNA hybrids formed at transcriptional pause sites to promote Xrn2-dependent termination. *Mol. Cell* **42**, 794–805 (2011).
- Cristini, A., Groh, M., Kristiansen, M. S. & Gromak, N. RNA/DNA hybrid interactome identifies DXH9 as a molecular player in transcriptional termination and R-loop-associated DNA damage. *Cell Rep.* **23**, 1891–1905 (2018).
- Chakravarti, D., LaBella, K. A. & DePinho, R. A. Telomeres: history, health, and hallmarks of aging. *Cell* **184**, 306–322 (2021).
- Morin, G. B. The human telomere terminal transferase enzyme is a ribonucleoprotein that synthesizes TTAGGG repeats. *Cell* **59**, 521–529 (1989).
- Nakamura, T. M. et al. Telomerase catalytic subunit homologs from fission yeast and human. *Science* **277**, 955–959 (1997).
- Meyerson, M. et al. hEST2, the putative human telomerase catalytic subunit gene, is up-regulated in tumor cells and during immortalization. *Cell* **90**, 785–795 (1997).
- Weinrich, S. L. et al. Reconstitution of human telomerase with the template RNA component hTR and the catalytic protein subunit hTERT. *Nat. Genet.* **17**, 498–502 (1997).
- Cong, Y. & Shay, J. W. Actions of human telomerase beyond telomeres. *Cell Res* **18**, 725–732 (2008).
- Martinez, P. & Blasco, M. A. Telomeric and extra-telomeric roles for telomerase and the telomere-binding proteins. *Nat. Rev. Cancer* **11**, 161–176 (2011).
- Maida, Y. et al. An RNA-dependent RNA polymerase formed by TERT and the RMRP RNA. *Nature* **461**, 230–235 (2009).
- Maida, Y. et al. Involvement of telomerase reverse transcriptase in heterochromatin maintenance. *Mol. Cell. Biol.* **34**, 1576–1593 (2014).
- Yasukawa, M. et al. CDK1 dependent phosphorylation of hTERT contributes to cancer progression. *Nat. Commun.* **11**, 1557 (2020).
- Matsuda, Y. et al. Phosphorylation of hTERT at threonine 249 is a novel tumor biomarker of aggressive cancer with poor prognosis in multiple organs. *J. Pathol.* <https://doi.org/10.1002/path.5876> (2022).
- Maida, Y., Yasukawa, M. & Masutomi, K. De novo RNA synthesis by RNA-dependent RNA polymerase activity of telomerase reverse transcriptase. *Mol. Cell. Biol.* **36**, 1248–1259 (2016).
- Raghuveer, M., Geelen, D., Majerova, E. & Decottignies, A. NHP2 downregulation counteracts hTR-mediated activation of the DNA damage response at ALT telomeres. *EMBO J.* **40**, e106336 (2021).
- Jeitany, M. et al. A preclinical mouse model of glioma with an alternative mechanism of telomere maintenance (ALT). *Int. J. Cancer* **136**, 1546–1558 (2015).
- Cohen, S. B. et al. Protein composition of catalytically active human telomerase from immortal cells. *Science* **315**, 1850–1853 (2007).
- Cohen, S. B. & Reddel, R. R. A sensitive direct human telomerase activity assay. *Nat. Methods* **5**, 355–360 (2008).
- Bryan, T. M., Englezou, A., Gupta, J., Bacchetti, S. & Reddel, R. R. Telomere elongation in immortal human cells without detectable telomerase activity. *EMBO J.* **14**, 4240–4248 (1995).
- Bryan, T. M., Englezou, A., Dalla-Pozza, L., Dunham, M. A. & Reddel, R. R. Evidence for an alternative mechanism for maintaining telomere length in human tumors and tumor-derived cell lines. *Nat. Med.* **3**, 1271–1274 (1997).
- Stewart, S. A. et al. Telomerase contributes to tumorigenesis by a telomere length-independent mechanism. *Proc. Natl Acad. Sci. USA* **99**, 12606–12611 (2002).
- Kilian, A. et al. Isolation of a candidate human telomerase catalytic subunit gene, which reveals complex splicing patterns in different cell types. *Hum. Mol. Genet.* **6**, 2011–2019 (1997).
- Yi, X., Shay, J. W. & Wright, W. E. Quantitation of telomerase components and hTERT mRNA splicing patterns in immortal human cells. *Nucleic Acids Res.* **29**, 4818–4825 (2001).
- Hrdlickova, R., Nehyba, J. & Bose, H. R. Jr. Alternatively spliced telomerase reverse transcriptase variants lacking telomerase activity stimulate cell proliferation. *Mol. Cell. Biol.* **32**, 4283–4296 (2012).
- Yeager, T. R. et al. Telomerase-negative immortalized human cells contain a novel type of promyelocytic leukemia (PML) body. *Cancer Res.* **59**, 4175–4179 (1999).
- Li, P. et al. Phase transitions in the assembly of multivalent signalling proteins. *Nature* **483**, 336–340 (2012).
- Banani, S. F., Lee, H. O., Hyman, A. A. & Rosen, M. K. Biomolecular condensates: organizers of cellular biochemistry. *Nat. Rev. Mol. Cell Biol.* **18**, 285–298 (2017).
- Oldfield, C. J. & Dunker, A. K. Intrinsically disordered proteins and intrinsically disordered protein regions. *Annu. Rev. Biochem.* **83**, 553–584 (2014).
- Saitoh, N. et al. Proteomic analysis of interchromatin granule clusters. *Mol. Biol. Cell* **15**, 3876–3890 (2004).
- Spector, D. L. & Lamond, A. I. Nuclear speckles. *Cold Spring Harb. Perspect. Biol.* **3**, a000646 (2011).

35. Fedorov, O. et al. Specific CLK inhibitors from a novel chemotype for regulation of alternative splicing. *Chem. Biol.* **18**, 67–76 (2011).
36. Tripathi, V. et al. The nuclear-retained noncoding RNA MALAT1 regulates alternative splicing by modulating SR splicing factor phosphorylation. *Mol. Cell* **39**, 925–938 (2010).
37. Azzalin, C. M., Reichenbach, P., Khoraiuli, L., Giulotto, E. & Lingner, J. Telomeric repeat containing RNA and RNA surveillance factors at mammalian chromosome ends. *Science* **318**, 798–801 (2007).
38. Arora, R. et al. RNaseH1 regulates TERRA-telomeric DNA hybrids and telomere maintenance in ALT tumour cells. *Nat. Commun.* **5**, 5220 (2014).
39. Chu, H. P. et al. TERRA RNA antagonizes ATRX and protects telomeres. *Cell* **170**, 86–101.e116 (2017).
40. Graf, M. et al. Telomere length determines TERRA and R-loop regulation through the cell cycle. *Cell* **170**, 72–85.e14 (2017).
41. Schweingruber, C., Rufener, S. C., Zund, D., Yamashita, A. & Muhlemann, O. Nonsense-mediated mRNA decay - mechanisms of substrate mRNA recognition and degradation in mammalian cells. *Biochim. Biophys. Acta* **1829**, 612–623 (2013).
42. Doench, J. G. et al. Optimized sgRNA design to maximize activity and minimize off-target effects of CRISPR-Cas9. *Nat. Biotechnol.* **34**, 184–191 (2016).
43. Li, W. et al. MAGeCK enables robust identification of essential genes from genome-scale CRISPR/Cas9 knockout screens. *Genome Biol.* **15**, 554 (2014).
44. Garcia-Higuera, I. et al. Interaction of the Fanconi anemia proteins and BRCA1 in a common pathway. *Mol. Cell* **7**, 249–262 (2001).
45. Niedernhofer, L. J., Lalai, A. S. & Hoeijmakers, J. H. Fanconi anemia (cross)linked to DNA repair. *Cell* **123**, 1191–1198 (2005).
46. Ray Chaudhuri, A. & Nussenzweig, A. The multifaceted roles of PARP1 in DNA repair and chromatin remodelling. *Nat. Rev. Mol. Cell Biol.* **18**, 610–621 (2017).
47. Sakai, W. et al. Secondary mutations as a mechanism of cisplatin resistance in BRCA2-mutated cancers. *Nature* **451**, 1116–1120 (2008).
48. Taniguchi, T. et al. Disruption of the Fanconi anemia-BRCA pathway in cisplatin-sensitive ovarian tumors. *Nat. Med.* **9**, 568–574 (2003).
49. Mender, I., Gryaznov, S., Dikmen, Z. G., Wright, W. E. & Shay, J. W. Induction of telomere dysfunction mediated by the telomerase substrate precursor 6-thio-2'-deoxyguanosine. *Cancer Discov.* **5**, 82–95 (2015).
50. Bhatia, V. et al. BRCA2 prevents R-loop accumulation and associates with TREX-2 mRNA export factor PCID2. *Nature* **511**, 362–365 (2014).
51. Garcia-Rubio, M. L. et al. The Fanconi anemia pathway protects genome integrity from R-loops. *PLoS Genet.* **11**, e1005674 (2015).
52. Vohhodina, J. et al. BRCA1 binds TERRA RNA and suppresses R-Loop-based telomeric DNA damage. *Nat. Commun.* **12**, 3542 (2021).
53. Sanz, L. A. & Chedin, F. High-resolution, strand-specific R-loop mapping via S9.6-based DNA-RNA immunoprecipitation and high-throughput sequencing. *Nat. Protoc.* **14**, 1734–1755 (2019).
54. Perrem, K., Colgin, L. M., Neumann, A. A., Yeager, T. R. & Reddel, R. R. Coexistence of alternative lengthening of telomeres and telomerase in hTERT-transfected GM847 cells. *Mol. Cell. Biol.* **21**, 3862–3875 (2001).
55. Grobelny, J. V., Kulp-McEliece, M. & Broccoli, D. Effects of reconstitution of telomerase activity on telomere maintenance by the alternative lengthening of telomeres (ALT) pathway. *Hum. Mol. Genet.* **10**, 1953–1961 (2001).
56. Cerone, M. A., Londono-Vallejo, J. A. & Bacchetti, S. Telomere maintenance by telomerase and by recombination can coexist in human cells. *Hum. Mol. Genet.* **10**, 1945–1952 (2001).
57. Venteicher, A. S. et al. A human telomerase holoenzyme protein required for Cajal body localization and telomere synthesis. *Science* **323**, 644–648 (2009).
58. Azzalin, C. M. & Lingner, J. Telomere functions grounding on TERRA firma. *Trends Cell Biol.* **25**, 29–36 (2015).
59. Tong, A. S. et al. ATM and ATR signaling regulate the recruitment of human telomerase to telomeres. *Cell Rep.* **13**, 1633–1646 (2015).
60. Perera, O. N. et al. Telomerase promotes formation of a telomere protective complex in cancer cells. *Sci. Adv.* **5**, eaav4409 (2019).
61. Xi, L. & Cech, T. R. Inventory of telomerase components in human cells reveals multiple subpopulations of hTR and hTERT. *Nucleic Acids Res.* **42**, 8565–8577 (2014).
62. Chen, L. et al. R-ChIP Using Inactive RNase H reveals dynamic coupling of R-loops with transcriptional pausing at gene promoters. *Mol. Cell* **68**, 745–757.e745 (2017).
63. Skourti-Stathaki, K., Kamieniarz-Gdula, K. & Proudfoot, N. J. R-loops induce repressive chromatin marks over mammalian gene terminators. *Nature* **516**, 436–439 (2014).
64. Lu, R. & Pickett, H. A. Telomeric replication stress: the beginning and the end for alternative lengthening of telomeres cancers. *Open Biol.* **12**, 220011 (2022).
65. Silva, B. et al. FANCM limits ALT activity by restricting telomeric replication stress induced by deregulated BLM and R-loops. *Nat. Commun.* **10**, 2253 (2019).
66. Lord, C. J. & Ashworth, A. BRCAness revisited. *Nat. Rev. Cancer* **16**, 110–120 (2016).

Publisher's note Springer Nature remains neutral with regard to jurisdictional claims in published maps and institutional affiliations.

Springer Nature or its licensor (e.g. a society or other partner) holds exclusive rights to this article under a publishing agreement with the author(s) or other rightsholder(s); author self-archiving of the accepted manuscript version of this article is solely governed by the terms of such publishing agreement and applicable law.

© The Author(s), under exclusive licence to Springer Nature Limited 2024

Methods

Our research complies with the relevant ethical regulations. All experiments using mice and recombinant DNA were performed in accordance with the study protocols approved by the Ethics Committee and the Recombinant DNA Experiment Committee of National Cancer Center (2015-187, B60M7-20 and B60M8-22) and the Animal Care and Use Committee of Kanazawa University (2017-050) and Tohoku University (2019NiA-001).

Cell culture and reagents

The human osteosarcoma cell line U2OS (300364, CLS) was cultured in DMEM/F-12 with 5% heat-inactivated fetal bovine serum (IFS). The SV40 transformed human fibroblast cell line VA-13 (RCB0251, RIKEN BRC), the human osteosarcoma cell line Saos-2 (RCB0428, RIKEN BRC), the human cervical carcinoma cell line HeLa (CVCL_0030, ATCC), the human hepatocellular carcinoma cell line Huh-7 (JCRB0403, JCRB Cell Bank), the human ovarian cancer cell line TOV-21G (CVCL_3613, ATCC), the FANCF transduced human ovarian cancer cell line TOV-21GFANCF⁴⁸, the BRCA2-mutated human pancreatic cancer cell line Capan-1 (HTB-79, ATCC), the BRCA2-restored Capan-1 clones (C2-1 and C2-2)⁴⁷, and the SV40 transformed human embryonic kidney cell line HEK-293T (CVCL_0063, ATCC) were cultured in DMEM with 10% IFS. To synchronize cells to mitotic phase, the cells were treated with medium containing 0.1 $\mu\text{g ml}^{-1}$ nocodazole overnight. A CDK1 inhibitor RO-3306, CPT and nocodazole were purchased from Merck. A telomerase inhibitor 6-thio-dG and a CLK1 inhibitor KH-CB19 were purchased from Selleck Chemicals.

Antibodies

Anti-hTERT mouse mAbs (clones 10E9-2 and 2E4-2)^{15,18} and an anti-p-hTERT mouse mAb (clone TpMab-3)¹⁷ were previously generated, and the specificity was evaluated. An anti-p-hTERT mouse monoclonal antibody (mAb; clone TpMab-35) was newly generated in this study. An anti-hTERT mouse mAb (clone 2E4-2, 1:200), anti-p-hTERT mouse mAbs (clones TpMab-3 and TpMab-35, 1:200), an anti-phospho-SR proteins mouse mAb (1H4, Merck, MABE50, 1:800), an anti-SF3B1 mAb (clone I6, MBL, D221-3, 1:1,000), anti-U2AF1 polyclonal antibodies (pAbs; MBL, RN085PW, 1:1,000), anti-histone H2A rabbit pAbs (Cell Signaling Technology, 2578S, 1:1,000), an anti-BRCA2 mouse mAb (Ab-1, Merck, OP95, 1:250), an anti-dsRNA mouse mAb (J2, SCICON, 10010200, 1:200), an anti-RNA-DNA hybrid mouse mAb (S9.6, Merck, MABE1095, 1:5,000) and an anti-dsDNA mouse mAb (HYB331-01, Santa Cruz Biotechnology, sc-58749, 1:5,000) were used for IB. An anti-hTERT mAb (clone 10E9-2, MBL, M216-3, 1:100), an anti-p-hTERT mouse mAb (clone TpMab-3, 1:50), anti-hTERT sheep pAbs (abx120550, Abnova, 1:50) and an anti-RNA-DNA hybrid mouse mAb (S9.6, Merck, MABE1095, 1:100), were used for IP. Anti-p-hTERT mouse mAbs (clones TpMab-3 and TpMab-35, 1:100), an anti-SC-35 mAb (against SRRM2) (SC-35, Merck, S4045, 1:2,000), an anti- γ H2AX rabbit mAb (20E3, Cell Signaling Technology, 9718, 1:500), an anti-PML rabbit mAb (EPRI6792, abcam, ab179466, 1:500) and anti-TRF2 goat pAbs (Novus Biologicals, NB100-56694, 1:250) were used for IIF staining.

TpMab-35 was established as described previously¹⁷. Briefly, female BALB/cAJcl mice (6 weeks old) were purchased from CLEA Japan. They were maintained in specific pathogen-free (SPF) rooms at 20 °C, 50% humidity and 11 h/13 h light/dark cycle condition. The Animal Care and Use Committee of Tohoku University approved all animal experiments. To develop mAbs against p-hTERT, 100 μg of keyhole limpet hemocyanin (KLH)-conjugated hTERT phosphopeptide₂₄₄CEPERpTPVGQG₂₅₄ (Eurofins Genomics) was immunized intraperitoneally (i.p.) with Imject Alum (Thermo Fisher Scientific) into one BALB/c mouse. The procedure included three additional immunizations of 100 μg , followed by a final booster intraperitoneal injection of 100 μg two days before its spleen cells were harvested. The harvested spleen cells were subsequently fused with P3U1 cells, using polyethylene glycol

1500 (PEG1500; Roche Diagnostics). Then, hybridomas were grown in an RPMI-1640 medium, supplemented with 10% heat-inactivated FBS, 100 units ml^{-1} penicillin, 100 $\mu\text{g ml}^{-1}$ streptomycin, 0.25 $\mu\text{g ml}^{-1}$ amphotericin B, and hypoxanthine/aminopterin/thymidine (HAT) for the selection (Thermo Fisher Scientific). Cultured supernatants were finally screened using enzyme-linked immunosorbent assay (ELISA) for the detection of hTERT phosphopeptide and nonphosphopeptide¹⁶. The clone TpMab-35, which is specific for the p-hTERT peptide, was finally established.

Indirect immunofluorescence staining

Cells were fixed with 4% formaldehyde in PBS, permeabilized with 0.2% TritonX-100 in PBS, and blocked with 2% bovine serum albumin in PBS. The cells were incubated with 10 $\mu\text{g ml}^{-1}$ of anti-phospho-hTERT mouse mAbs (clones TpMab-3 and TpMab-35), 10 $\mu\text{g ml}^{-1}$ of an anti-hTERT mouse mAb (clone 2E4-2), 1:2,000 dilution of an anti-SC-35 mAb (against SRRM2; SC-35, Merck), 1:200 dilution of an anti-phospho-SR proteins mouse mAb (1H4, Merck), 1:500 dilution of an anti- γ H2AX rabbit mAb (20E3, Cell Signaling Technology), 1:500 dilution of an anti-PML rabbit mAb (EPRI6792, abcam) and/or 1:250 dilution of anti-TRF2 goat pAbs (Novus Biologicals), followed by incubation in the presence of Alexa488- or Alexa568-labelled secondary antibody (1:1,000; Thermo Fisher Scientific). The nuclei were stained with Hoechst 33342 (NucBlue; Thermo Fisher Scientific).

TERRA RNA-FISH

The PNA probe against TERRA RNAs (TelC-FITC probe) was obtained from Panagene. Cells were fixed with 4% formaldehyde in PBS and permeabilized with 0.5% TritonX-100 in PBS. For a control sample, the cells were preincubated with 100 $\mu\text{g ml}^{-1}$ of RNase A for 20 min at 37 °C. After blocking with 2% BSA (Merck) in PBS, the cells were incubated with the primary antibody, followed by an incubation in the presence of an Alexa568-labelled secondary antibody (1:1,000; Thermo Fisher Scientific). The telomeric PNA probe was diluted at 1:100 in 60% formamide and boiled for 10 min at 85 °C. Cells were refixed with 4% formaldehyde in PBS and then hybridized with a hybridization solution containing the FITC-labelled telomeric PNA probe at room temperature for 2 h. The nuclei were stained with Hoechst 33342 (NucBlue; Thermo Fisher Scientific).

IP-IB of hTERT

Cells were lysed in Lysis Buffer A (0.5% NP-40, 20 mM Tris-HCl (pH 7.4) and 150 mM NaCl). After sonication for 10 seconds, lysates were centrifuged at 21,000g at 4 °C for 15 min and collect the supernatant. Lysate from 1×10^7 cells (Fig. 1) or 1 mg of lysate (Figs. 3 and 5) were pre-absorbed with 40 μl of Pierce Protein A Plus Agarose (Thermo Fisher Scientific) for 30 min at 4 °C. Pre-absorbed lysate was mixed with 10 μg of an anti-hTERT mAb (clone 10E9-2) and 40 μl of Pierce Protein A Plus Agarose, and incubated overnight at 4 °C. Immune complexes were washed three times with Lysis Buffer A and eluted in 2 \times SDS loading buffer (2% β -mercaptoethanol, 20% glycerol, 4% SDS and 100 mM Tris-HCl (pH 6.8)) with heating at 95 °C for 5 min, and then subjected to SDS-PAGE in 8% polyacrylamide gels. After electrophoresis under reducing conditions, bands of protein were transferred to nitrocellulose membranes (Amersham; Cytiva). After blocking with 5% skimmed milk prepared in TBS-T (Tween-20, 0.1%) or Immobilon Signal Enhancer (Merck), the membrane was incubated with an anti-hTERT mouse mAb (clone 2E4-2) or anti-p-hTERT mouse mAbs (clones TpMab-3 and TpMab-35), followed by incubation in the presence of Mouse TrueBlot ULTRA Anti-Mouse Ig horseradish peroxidase (HRP; Rockland).

IP-RdRP assay

hTERT and p-hTERT proteins were immunoprecipitated from human cell lines as described for the IP-IB assay with an anti-hTERT mAb (clone 10E9-2) and an anti-p-hTERT mAb (clone TpMab-3), respectively. The

bead suspension with immune complexes was washed four times with 1× acetate buffer (10 mM HEPES-KOH (pH 7.8), 100 mM potassium acetate, and 4 mM MgCl₂) containing 10% glycerol, 0.1% Triton-X and 0.06× Complete EDTA-free (Roche Diagnostics), and once with AGC solution (1× acetate buffer containing 10% glycerol and 0.02% CHAPS) containing 2 mM CaCl₂. The bead suspension was treated with 0.25 units per μl Micrococcal Nuclease (MNase; Takara Bio) at 25 °C for 15 min. Immunoprecipitants were subsequently washed twice with AGC solution containing 3 mM EGTA and once with 1× acetate buffer containing 0.02% CHAPS. Reaction mixture (40 μl) was prepared by combining 20 μl of the bead suspension with 6 μl of [α -³²P] UTP (3,000 Ci per mmol) and 25 ng μl⁻¹ (final concentration) of RNA template, and incubated at 32 °C for 2 h. The following RNA templates were used: DN3AS (5'-GGGAUCAUGUGGGUCCUAUUACAUUUAAACCCA-3', used in Figs. 2, 3 and 5 and Extended Data Fig. 4j) and TERRA (5'-(GUUAGG)₈-3', used in Fig. 4). These RNAs have hydroxyl groups at both the 5' and 3' ends. The final concentrations of ribonucleotides were 1 mM ATP, 0.2 mM GTP, 10 μM UTP and 0.2 mM CTP. The resulting products were treated with Proteinase K to stop the reaction, purified several times with phenol/chloroform until the white interface disappeared and precipitated using ethanol. The RdRP products were treated with RNase I (2 U, Promega) at 37 °C for 2 h to digest single-stranded RNAs completely, followed by Proteinase K treatment, phenol/chloroform purification and ethanol precipitation. The products were electrophoresed in a 15% polyacrylamide gel containing 7 M urea, and detected by autoradiography.

Direct telomerase assay

For the direct telomerase assay, we modified the original methods^{21,22}. TERT protein was immunoprecipitated from human cell lines as described for the IP-IB assay with incubation on ice for 30 min without sonication. Immune complexes were washed three times with Lysis buffer A, and then suspended in 30 μl of TRAP lysis buffer (10 mM Tris-HCl (pH 7.5), 1 mM MgCl₂, 1 mM EGTA, 0.5% CHAPS, 10% glycerol, 100 μM Pefabloc SC, and 0.035% 2-mercaptoethanol). The direct telomerase assay was carried out with 10 μl of the suspension and 40 μl of reaction mixture (2.5 μl of [α -³²P] dGTP (6000 Ci/mmol), 50 mM Tris-HCl (pH 8.0), 50 mM KCl, 1 mM MgCl₂, 1.25 mM Spermidine, 5 mM 2-mercaptoethanol, 2.5 mM dTTP, 2.5 mM dATP, 25 μM dGTP and 2.5 μM a5 primer (5'-TTAGGGTTAGGGTTAGCGTTA-3')) by incubation at 37 °C for 2 h. The products were purified with phenol/chloroform and precipitated using ethanol. The products were electrophoresed in a 10% polyacrylamide gel containing 7 M urea and detected by autoradiography.

Telomere length measurement

To measure telomere length by Southern blotting analysis, hTERT-CRISPR clones were cultured and their population doublings were calculated. Genomic DNAs (gDNAs) were isolated with the GenElute Mammalian genomic DNA miniprep kit (Merck) according to the manufacturer's instructions. The isolated gDNAs were then digested with *Hinf*I and *Afa*I, electrophoresed in a 0.8% agarose gel and hybridized with a ³²P-labelled telomeric (CCCTAA)₃ probe as described previously⁶⁷.

Semi-quantitative and quantitative reverse transcription PCR

Total RNA was isolated from cells using TRIzol (Thermo Fisher Scientific) and treated with RQ1 DNase (Promega). cDNA was synthesized using 500 ng of total RNA with oligo (dT)₁₂₋₁₈ primer (Thermo Fisher Scientific), random hexamers (Thermo Fisher Scientific) and one of reverse transcriptases, PrimeScript reverse transcriptase (Takara Bio), Superscript IV reverse transcriptase (Thermo Fisher Scientific) or Superscript IV VILO master mix (Thermo Fisher Scientific), followed by PCR analyses. Semi-quantitative PCR analysis was performed using Ex-Taq DNA polymerase (TaKaRa Bio). qRT-PCR analysis was performed using Fast SYBR Green Master Mix (Thermo Fisher Scientific) and

QuantStudio 5 Real-Time PCR System (Thermo Fisher Scientific). All data of qRT-PCR analysis were normalized by the data of GAPDH mRNA levels. For determination of RNA levels in NSs, the data of qRT-PCR analysis were normalized by the amount of RNAs (Fig. 3d). The sequences of the primers used in this study are described in Supplementary Table 1.

Transfection of siRNA

Cells were transfected with siRNAs using lipofectamine 2000 (Thermo Fisher Scientific) according to the manufacturer's instructions. To suppress hTERT expression efficiently, we treated the cells with siRNAs specific for hTERT twice for IIF analysis. The sequences of siRNAs were as follows: siTERT#1, GUGUCUGUGCCCGGAGAATT; siTERT#2, GCAUUGGAAUCAGACAGCATT. MISSION siRNA Universal Negative Control #1 (Merck) was used as a negative control. The following Silencer Select siRNAs (Thermo Fisher Scientific) were used: siBRCA1 (s457, s458), siBRCA2 (s2083, s2085), siFANCD2 (s4988, 4989), siFANCE (s4992), siFANCF (s5015), siPARP1 (s1098, s1099).

Genome editing using CRISPR-Cas9

Recombinant Cas9 protein (TrueCut Cas9 Protein v2; Thermo Fisher Scientific) and *TERT*-specific gRNA (TrueGuide synthetic guide RNA, Thermo Fisher Scientific, CRISPR117444_SGM) were premixed and transfected into U2OS cells using lipofectamine CRISPRMAX Cas9 transfection reagent (Thermo Fisher Scientific) according to the manufacturer's instructions. After 4 days' incubation, a single cell was cloned. The transfection and clonal selection process were repeated once more. Genomic DNA was extracted with the GenElute Mammalian genomic DNA miniprep kit (Merck) according to the manufacturer's instructions. Presence of mutation in single-cell clones was confirmed by PCR amplification and Sanger sequencing using primers 5'-TTGAATTCGAACCATAGCGTCAGGGAGG-3' and 5'-TTGAATTCGAACCATAGCGTCAGGGAGG-3'.

RNA-seq and data analysis

RNA sequence library preparation, sequencing, mapping, gene expression and GO enrichment analysis were performed by DNAFORM. Qualities of total RNA were assessed by Bioanalyzer (Agilent) to ensure that RIN (RNA integrity number) is over 7.0. Sequencing cDNA libraries (RNA-seq libraries) were prepared using SMARTer stranded Total RNA Sample Prep Kit-HI Mammalian (Takara Bio) according to the manufacturer's instruction. RNA-seq libraries were sequenced using paired end reads on a NextSeq 500 instrument (Illumina). Obtained raw reads were trimmed and quality-filtered using the Trim Galore! (version 0.6.4_dev), Trimmomatic (version 0.39) and cutadapt (version 2.10) software. Trimmed reads were then mapped to the human GRCh38 genome using STAR (version 2.7.9a)⁶⁸. Reads on annotated genes were counted using featureCounts (version 2.0.1)⁶⁹. FPKM values were calculated from mapped reads by normalizing to total counts and transcript. Differentially expressed genes were detected using the DESeq2 package (version 1.20.0). The list of differentially expressed genes was used for clustering analysis with MBoCluster.Seq package⁷⁰ and GO enrichment analysis with clusterProfiler package⁷¹.

Recombinant human hTERT

rhTERT and AS variant proteins were produced by Fujifilm Wako Pure Chemical using a baculovirus expression system. The *TERT* and AS variant genes were synthesized and inserted into a transfer vector. The transfer vector was cotransfected with baculovirus DNA into Sf9 cells. After incubation, the supernatant containing the recombinant baculovirus was harvested and then infected into expressSF+ cells for larger scale expression of recombinant proteins. The cell pellet was harvested and lysed in lysis buffer (0.5% NP-40, 20 mM Tris-HCl (pH 7.4), and 150 mM NaCl). After sonication for 10 seconds, lysates were centrifuged at 21,000g at 4 °C for 15 min and collect the supernatant. The recombinant hTERT and AS variant proteins were purified with an

anti-hTERT mAb (clone 10E9-2) and Pierce Protein A Plus Agarose from the supernatant and used for the IP-IB and IP-RdRP assays.

Generation of stable cell lines

Lentiviruses were created using the lentiviral vectors pLV-puro, pLV-puro-hTERT or pLV-puro-T249A, constructed by Vectorbuilder. T249A mutant, in which the threonine 249 of hTERT is replaced with alanine, are not phosphorylated and thus lack the RdRP activity¹⁶. After infection, polyclonal cell populations were purified by selection with puromycin ($2 \mu\text{g ml}^{-1}$) for 2 days.

Genome-wide CRISPR screening

Human Brunello CRISPR knockout pooled library lentiviral prep was obtained from Addgene (73179-LV)⁴². U2OS cells or the hTERT-CRISPR clone #2 (10^8 cells) were infected with the pooled lentivirus library at a multiplicity of infection of ~ 0.4 and >500 -fold coverage of the library. Forty-eight hours postinfection, cells were selected with puromycin ($2 \mu\text{g ml}^{-1}$). After 48 h selection, 4×10^7 cells were collected as a control sample (day 0 timepoint), and the others were seeded to start the screen. Every 3 days, 4×10^7 cells were passaged (~ 500 -fold coverage of the library). After 21 days of culture, 4×10^7 cells were harvested, and gDNAs were isolated from the cell pellets using the Blood and Cell Culture DNA Maxi Kit (Qiagen). sgRNA sequences were amplified from 200 μg of gDNA by 20 parallel PCR reactions (10 μg of gDNA per tube) using Q5 High-Fidelity DNA Polymerase (New England Biolabs). The resulting amplicons were mixed and purified by gel extraction using Wizard SV Gel and PCR Clean-Up System (Promega). Purified PCR products were subjected to high-throughput sequencing analysis with Illumina HiSeq 2500 platform (Illumina). The sequences of the primers used in this study are described in Supplementary Table 1. Sequencing data were analysed to obtain the read counts for each sgRNA and to generate a maximum-likelihood estimation (MLE) of gene essentiality score (β score) for each gene using the MAGeCK algorithm⁴³. Genes with a β score < -0.5 in hTERT-CRISPR groups, but with β score > -0.3 in U2OS groups were picked up as potential synthetic lethal genes. To predict the biological functions and pathways associated with the putative genes, GO analysis and KEGG pathway analysis were performed using the DAVID online tool (<https://david.ncicrf.gov/>).

Cell viability assay

For the colony formation assay, cells were seeded into 6-well plates at a density of 500 cells per well and subjected to transfection with the indicated siRNAs, treatment with chemical reagents or IR. After approximately 12 days, the cells were fixed with 4% formaldehyde in PBS, washed with PBS, and stained with 0.2% crystal violet in 20% methanol for 15 min at room temperature. After cells were washed with PBS twice, colony numbers were counted.

For MTT assay, cells were seeded into 96-well plates at a density of 10,000 cells per well and treated with chemical reagents. After 72 h incubation, cell viabilities were determined using Cell Proliferation Kit I MTT (Merck) according to the manufacturer's instructions.

Purification of nuclear speckles

To separate cells into cytoplasmic fraction and nuclear pellet, ~ 80 – 90% confluent cells in 150 mm dishes were lysed with 4 ml of HLB/NP40 buffer (10 mM Tris-HCl (pH 7.5), 10 mM NaCl, 0.5% NP40 and 2.5 mM MgCl_2) and incubated for 5 min on ice. After the incubation, 1 ml of HLB/NP40/Sucrose buffer (10 mM Tris-HCl (pH 7.5), 10 mM NaCl, 0.5% NP40, 2.5 mM MgCl_2 and 10% sucrose) was added under the lysate layer, followed isolation of nuclear pellet by centrifugation at 400g at 4 °C for 5 min. Isolated nuclear pellet was treated with 1% Triton X-100 in TM5 buffer (10 mM Tris-HCl (pH 7.4) and 5 mM MgCl_2) for 5 min on ice and the supernatant was removed by centrifugation at 700g at 4 °C for 5 min. The pellet was treated with 50 units of MNase (Takara Bio) at 4 °C for 30 min. The pellet was washed twice with TM5 buffer

containing 3 mM EGTA to inactivate MNase activity and 500 mM NaCl to remove nucleoplasmic extracts and chromatin. After centrifugation at 800g for 5 min, the pellet was treated with 500 mM NaCl as above. The final pellet was lysed in 800 μl of Lysis Buffer A. After sonication for 10 seconds, lysates were centrifuged at 21,000g at 4 °C for 15 min and the supernatant was collected as an NS-enriched fraction.

R-loop analysis by dot blot

HeLa cells were transfected with siRNAs. After 72 h incubation, gDNAs were isolated from the cells using the Blood and Cell Culture DNA Midi Kit (Qiagen). gDNA (2 μg) was dotted onto a Hybond N+ (Amersham) using a Bio-Dot Apparatus (Bio-Rad). The membrane was then cross-linked with ultraviolet (UV; 240 mJ cm^{-2}). After blocking with 5% skimmed milk prepared in TBS-T (Tween-20, 0.1%) and subsequently with SuperBlock buffer (Thermo Fisher Scientific), the membrane was incubated with an anti-RNA-DNA hybrid mouse mAb (S9.6, Merck) at 0.2 $\mu\text{g ml}^{-1}$ in SuperBlock buffer (Thermo Fisher Scientific) overnight at 4 °C, followed by incubation in the presence of HRP-labelled anti-mouse IgG secondary antibody (Jackson ImmunoResearch Laboratories).

Dot blot analysis of hTERT IP products

hTERT protein was immunoprecipitated from 1 mg of NS-enriched fraction as described for the IP-IB assay with an anti-hTERT mAb (clone 10E9-2) or an anti-p-hTERT mAb (clone TpMab-3). The bead suspension with immune complexes was washed four times with Lysis Buffer A and RNA co-immunoprecipitated with the p-hTERT immune complex was isolated using TRIzol (Thermo Fisher Scientific). The isolated RNA was treated with RQ1 RNase-Free DNase (Promega) and dotted onto a Hybond N+ (Amersham) using a Bio-Dot Apparatus (Bio-Rad). The membrane was then cross-linked with UV (120 mJ cm^{-2}) and then probed with ³²P-labelled synthetic oligonucleotides that were complementary to the sequence of TERRA RNA or ARRET RNA (TERRA RNA: 5'-(CCCTAA)₄-3'; ARRET RNA: 5'-(TTAGGG)₄-3').

For detection of dsRNAs, RNA co-immunoprecipitated with hTERT or p-hTERT was treated with DNase (Promega) and dotted onto the membrane as above. The membrane was then cross-linked with UV (240 mJ cm^{-2}). After blocking with 5% skimmed milk prepared in TBS-T (Tween-20, 0.1%) and subsequently with SuperBlock buffer (Thermo Fisher Scientific), the membrane was incubated with anti-dsRNA mouse mAb (J2, SCICONS) in SuperBlock buffer (Thermo Fisher Scientific) overnight at 4 °C, followed by incubation in the presence of HRP-labelled anti-mouse IgG secondary antibody (Jackson ImmunoResearch Laboratories). For prepare a control sample treated with dsRNA-specific RNase III, RNA was preincubated with 1 unit of RNase III (Thermo Fisher Scientific Inc.) for 2 h at 37 °C.

R-loop degradation assay

TERRA RNA oligonucleotide (5'-(GUUAGG)₈-3') and the complementary oligonucleotide DNA (5'-(CCTAAC)₈-3') were synthesized by Integrated DNA Technologies. To prepare TERRA RNA:DNA oligo duplex, 5'-³²P-labelled TERRA RNA and the complementary oligonucleotide DNA were annealed in annealing buffer (10 mM Tris-HCl (pH 7.5), 50 mM NaCl and 1 mM EDTA) at 80 °C for 5 min and slowly cooled to room temperature. hTERT immune complex was immunoprecipitated from 1 mg of NS-enriched fraction as described for the IP-IB assay with an anti-hTERT mAb (clone 10E9-2) or an anti-p-hTERT mAb (clone TpMab-3). The hTERT immune complex was washed three times and incubated with TERRA RNA:DNA hybrids in a buffer containing 50 mM NaCl, 10 mM Tris-HCl (pH 7.9), 10 mM MgCl_2 , 1 mM DTT, 1 mM ATP, 0.2 mM GTP, 0.2 mM UTP, and 0.2 mM CTP, and RNasin plus inhibitor for 2 h at 37 °C. The reaction samples were treated with Proteinase K to stop the reaction. After phenol/chloroform purification and ethanol precipitation, the reaction products were treated with 1 unit of RNase III (Thermo Fisher Scientific) at 37 °C for 1 h to digest dsRNAs generated by p-hTERT immune complex. The reaction products were subsequently

electrophoresed in a 10% polyacrylamide gel containing 7 M urea, and detected by autoradiography.

DNA–RNA hybrid immunoprecipitation (DRIP)

HeLa cells were transfected with siRNAs. After 72 h incubation, gDNAs were isolated from the cells using the Blood and Cell Culture DNA Midi Kit (Qiagen). gDNA (20 µg) were sonicated using Bioruptor (CosmoBio) at high power with 20 cycles (30 s on and 50 s off) in sonication buffer containing 10 mM Tris-HCl (pH 8.5) and 300 mM NaCl. The sonicated gDNAs were mixed with 5 µg of an anti-RNA–DNA hybrid mouse mAb (S9.6, Merck) and 40 µl of Pierce Protein A Plus Agarose and incubated overnight at 4 °C in DRIP buffer containing 50 mM Tris-HCl (pH 7.4), 150 mM NaCl, 5 mM EDTA and 1% NP-40. Immune complexes were washed with DRIP buffer, DRIP high buffer (50 mM Tris-HCl, pH 7.4, 500 mM NaCl, 5 mM EDTA, 1% NP-40), DRIP Li buffer (50 mM Tris-HCl, pH 8.0, 250 mM LiCl, 1 mM EDTA, 0.5% NP-40), and DRIP TE buffer (100 mM Tris-HCl pH 8.0, 10 mM EDTA), and then eluted in elution buffer containing Proteinase K (Takara Bio), 10 mM EDTA and 0.5% SDS by shaking at 37 °C for 30 min. After phenol/chloroform purification and ethanol precipitation, the DRIP products were treated with RQ1 DNase (Promega) to purify the RNA strand and subjected to qRT-PCR analysis with strand-specific primers. The sequences of the primers used in this study are described in Supplementary Table 1.

Xenotransplantation

Six-week-old male NOD/SCID mice (NOD/NCrCRL-Prkdc^{scid}) were purchased from Charles River Laboratories and used as recipients for xenotransplantation. They were maintained in SPF rooms at 20 °C, 50% humidity, and 12 h/12 h light/dark cycle condition. 1×10^5 cells were suspended in a mixture of serum-free medium and Matrigel (BD Biosciences; 1:1 volume). The mixture was injected subcutaneously through a 26-gauge needle into the right dorsal areas of anaesthetized NOD/SCID mice. We monitored tumour formation and tumour size every two or three days, and dissected out the tumours 10 weeks later. The study protocol was approved by the Kanazawa University Animal Care and Use Committee, and all procedures were performed in accordance with the guidelines and regulations of Kanazawa University.

Statistical analysis

Statistical significance was determined using two-tailed unpaired *t*-test or one-way ANOVA method with Dunnett correction for multiple comparisons. Data are presented as the mean \pm s.d. or s.e.m.

Reporting summary

Further information on research design is available in the Nature Portfolio Reporting Summary linked to this article.

Data availability

All sequencing datasets have been deposited at the Gene Expression Omnibus with accession codes [GSE226966](https://www.ncbi.nlm.nih.gov/geo/query/acc.cgi?acc=GSE226966) and [GSE226994](https://www.ncbi.nlm.nih.gov/geo/query/acc.cgi?acc=GSE226994). All the data supporting the findings of this study are available within the article and from the corresponding author upon reasonable request. Source data are provided with this paper.

References

67. Harley, C. B., Fitcher, A. B. & Greider, C. W. Telomeres shorten during ageing of human fibroblasts. *Nature* **345**, 458–460 (1990).

68. Dobin, A. et al. STAR: ultrafast universal RNA-seq aligner. *Bioinformatics* **29**, 15–21 (2013).
69. Liao, Y., Smyth, G. K. & Shi, W. featureCounts: an efficient general purpose program for assigning sequence reads to genomic features. *Bioinformatics* **30**, 923–930 (2014).
70. Si, Y., Liu, P., Li, P. & Brutnell, T. P. Model-based clustering for RNA-seq data. *Bioinformatics* **30**, 197–205 (2014).
71. Yu, G., Wang, L. G., Han, Y. & He, Q. Y. clusterProfiler: an R package for comparing biological themes among gene clusters. *OMICS* **16**, 284–287 (2012).

Acknowledgements

This work was supported in part by the Japan Society for the Promotion of Science KAKENHI (22K15550 to M.M., 20J00036 and 20H03438 to A.Y.), the Japan Science and Technology Agency (JPMJMS2022 to A.Y.) and several grants from the Japan Agency for Medical Research and Development: the P-CREATE grant (JP21cm0106584 and JP23ama221523 to M.M. and JP21cm0106115 to K.M.), the Practical Research for Innovation Cancer Control (JP20ck0106403 to K.M.), Basis for Supporting Innovative Drug Discovery and Life Science Research (BINDS; JP22ama121008 to Y.K.) and the Translational Research programme (JP24ym0126804 to M.M.). T.T. was supported by the Uehara Memorial Foundation and Tokai University Tokuda Memorial Cancer/Genome Basic Research Grant. This work was supported by the Center for Promotion of Translational Research, National Cancer Center Japan.

Author contributions

M.M., A.N., M.Y., S.U. and K.-I.F. performed biochemical and cellular experiments. T.Y. and S.K. performed animal experiments. T.U. and H.M. conducted bioinformatics analyses of CRISPR screening. Y.K. generated a phospho-specific monoclonal antibody against hTERT. T.T. provided FANC/BRCA mutant cell clones. N.S. supported purification of NSs. M.M., A.N., A.Y., Y.T., M.W. and K.M. designed the experiments and discussed the interpretation of the results. M.M., A.N. and K.M. wrote the paper.

Competing interests

The authors declare no competing interests.

Additional information

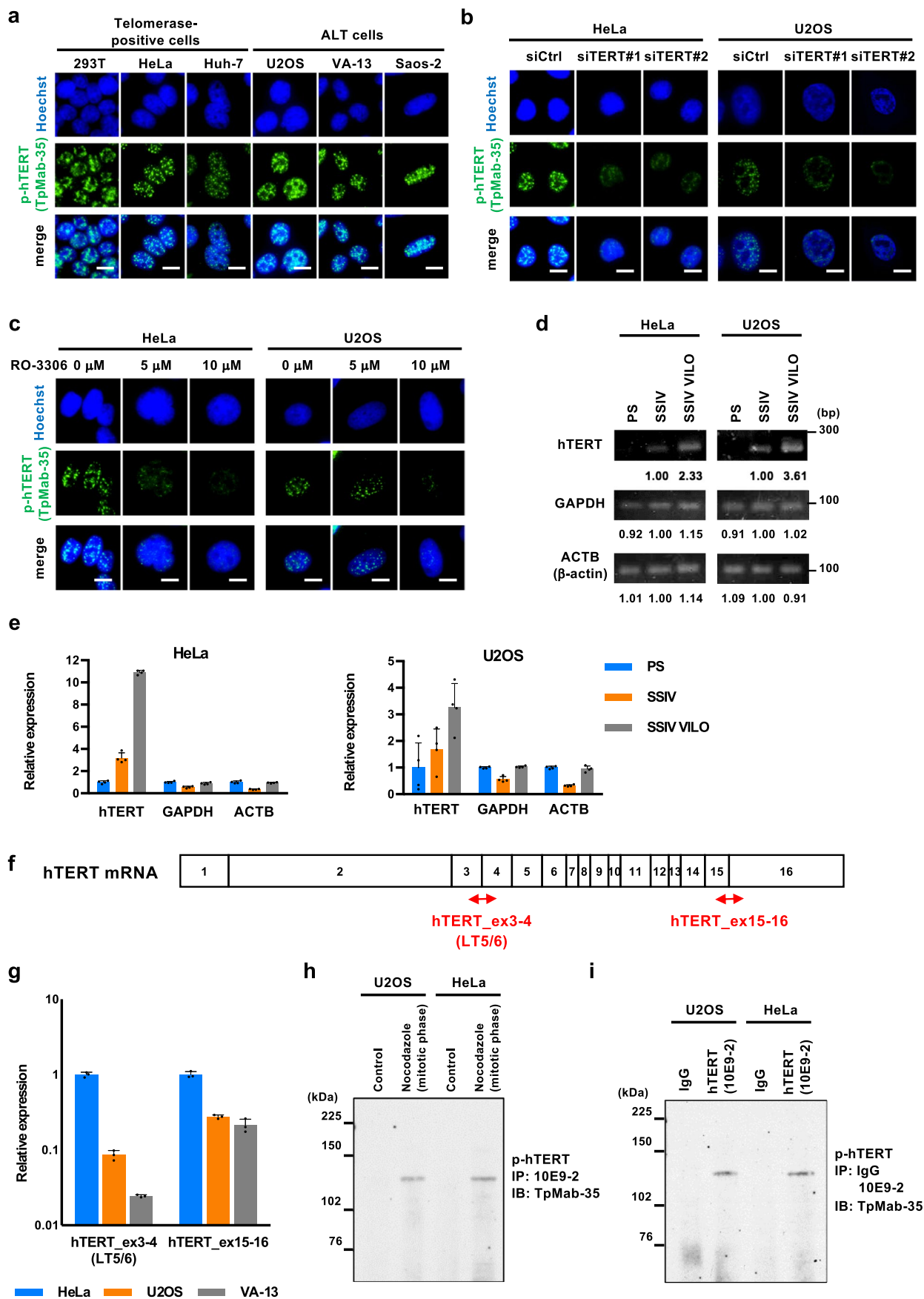
Extended data is available for this paper at <https://doi.org/10.1038/s41556-024-01427-6>.

Supplementary information The online version contains supplementary material available at <https://doi.org/10.1038/s41556-024-01427-6>.

Correspondence and requests for materials should be addressed to Kenkichi Masutomi.

Peer review information *Nature Cell Biology* thanks the anonymous reviewers for their contribution to the peer review of this work. Peer reviewer reports are available.

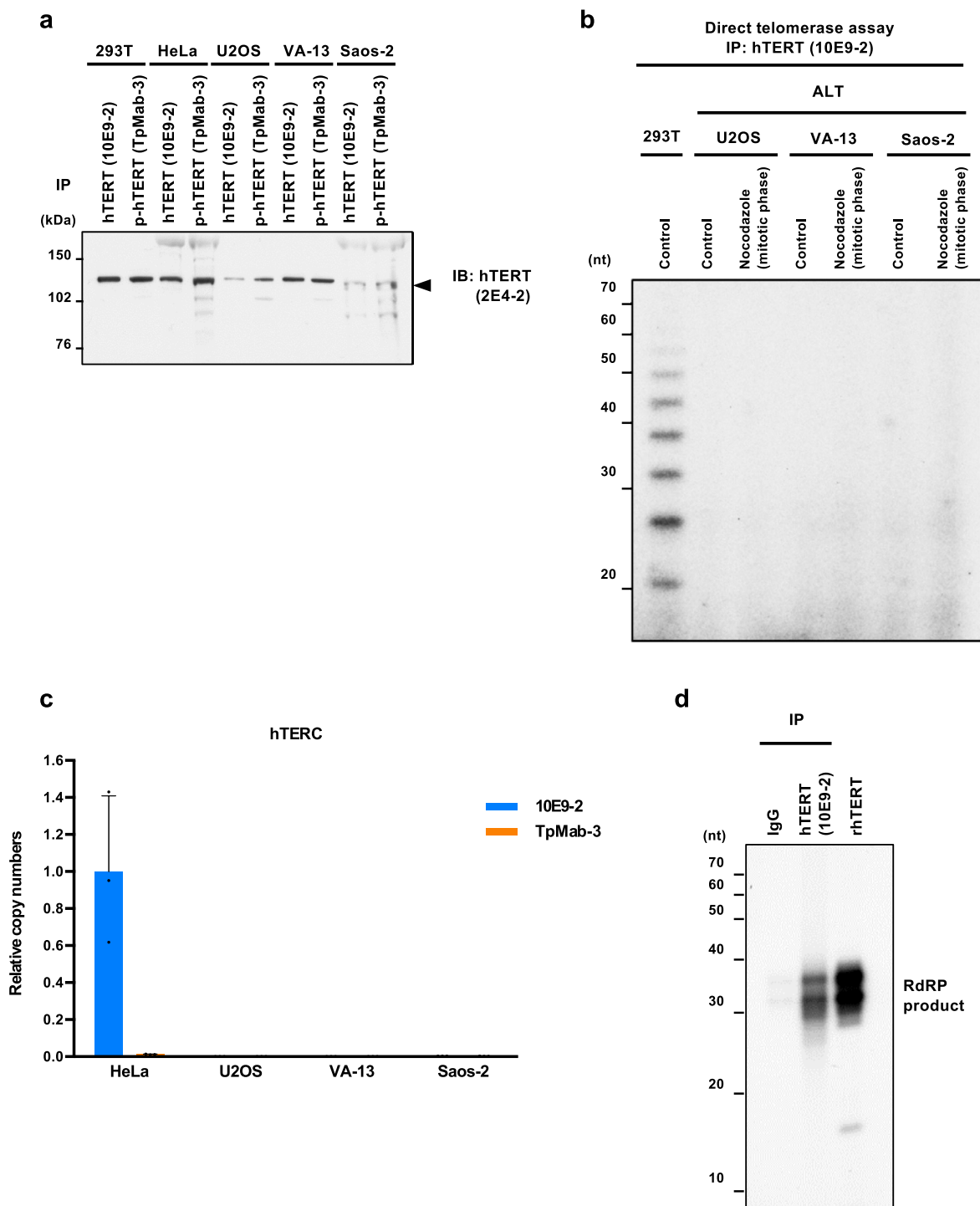
Reprints and permissions information is available at www.nature.com/reprints.



Extended Data Fig. 1 | See next page for caption.

Extended Data Fig. 1 | Detection of phosphorylated hTERT proteins and hTERT mRNAs in ALT cells. a, IIF imaging of p-hTERT. Telomerase-positive cell lines (293T, HeLa, and Huh-7 cells) and ALT cell lines (U2OS, VA-13, and Saos-2 cells) were immunostained with an anti-p-hTERT mouse mAb (TpMab-35). Scale bar, 10 μ m. **b, c**, IIF imaging of p-hTERT (TpMab-35) in HeLa and U2OS cells after treatment with hTERT siRNAs (**b**) and a CDK1 inhibitor (RO-3306) (**c**). Scale bar, 10 μ m. **d, e**, Comparison between reverse transcriptases for RT-PCR analysis (n = 4 independent experiments per group). cDNA was synthesized from total RNAs with PrimeScript (PS), Superscript IV (SSIV), or Superscript IV VILO.

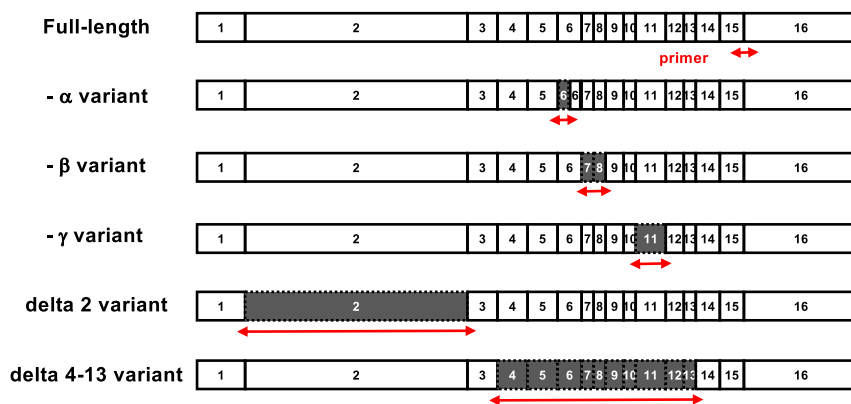
The relative expressions are noted below the panel (for **b**). **f**, Schematic diagram of hTERT mRNA. Arrows depict locations of primers used for quantitative RT-PCR analysis. **g**, Determination of hTERT mRNA levels by quantitative RT-PCR analysis using LT5/6 primer pairs or new primer pairs targeting the exon 15 and 16 junction of hTERT mRNA (n = 3 independent experiments per group). **h, i**, Detection of p-hTERT (TpMab-35) in U2OS and HeLa cells synchronized in mitosis with nocodazole. Data are presented as mean \pm SD (for **e, g**). Experiments were repeated three times (for **a, c**) and twice (for **b, d, h, i**) with similar results. Source numerical data and unprocessed blots are available in source data.



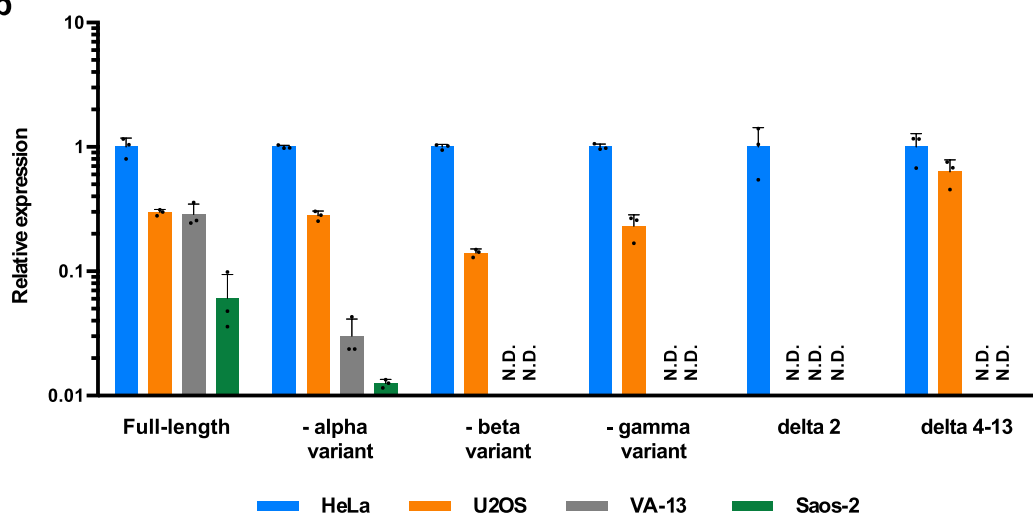
Extended Data Fig. 2 | Telomerase and RdRP activity in ALT cells. **a**, Detection of endogenous hTERT immunoprecipitated from the indicated cells with nocodazole treatment. **b**, Direct telomerase assay using hTERT proteins immunoprecipitated with an anti-hTERT mouse mAb (10E9-2) from the indicated mitotic cells treated with nocodazole. 293T cells are positive controls. **c**, quantitative RT-PCR analysis for hTERC associated with hTERT and p-hTERT

isolated with the 10E9-2 and the TpMab-3 antibodies from HeLa, U2OS, VA-13, and Saos-2 cells ($n = 3$ independent experiments per group). Data are presented as mean \pm SD. **d**, RdRP activity of endogenous hTERT immunoprecipitated from HeLa cells and a recombinant hTERT (rhTERT) protein. Experiments were repeated three times (for **a**, **b**, **d**) with similar results. Source numerical data and unprocessed blots are available in source data.

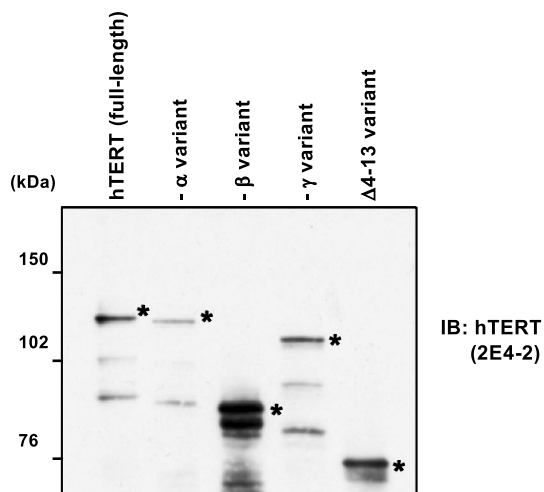
a



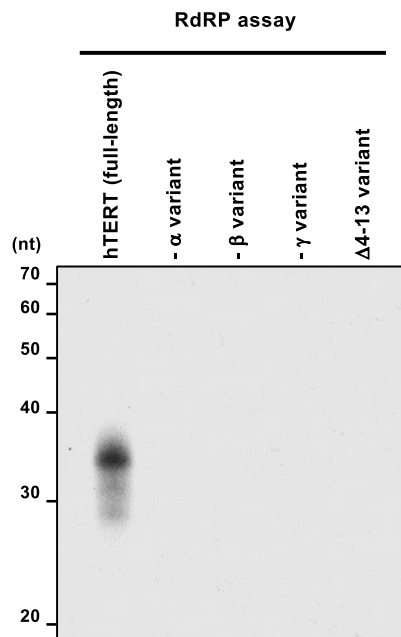
b



c



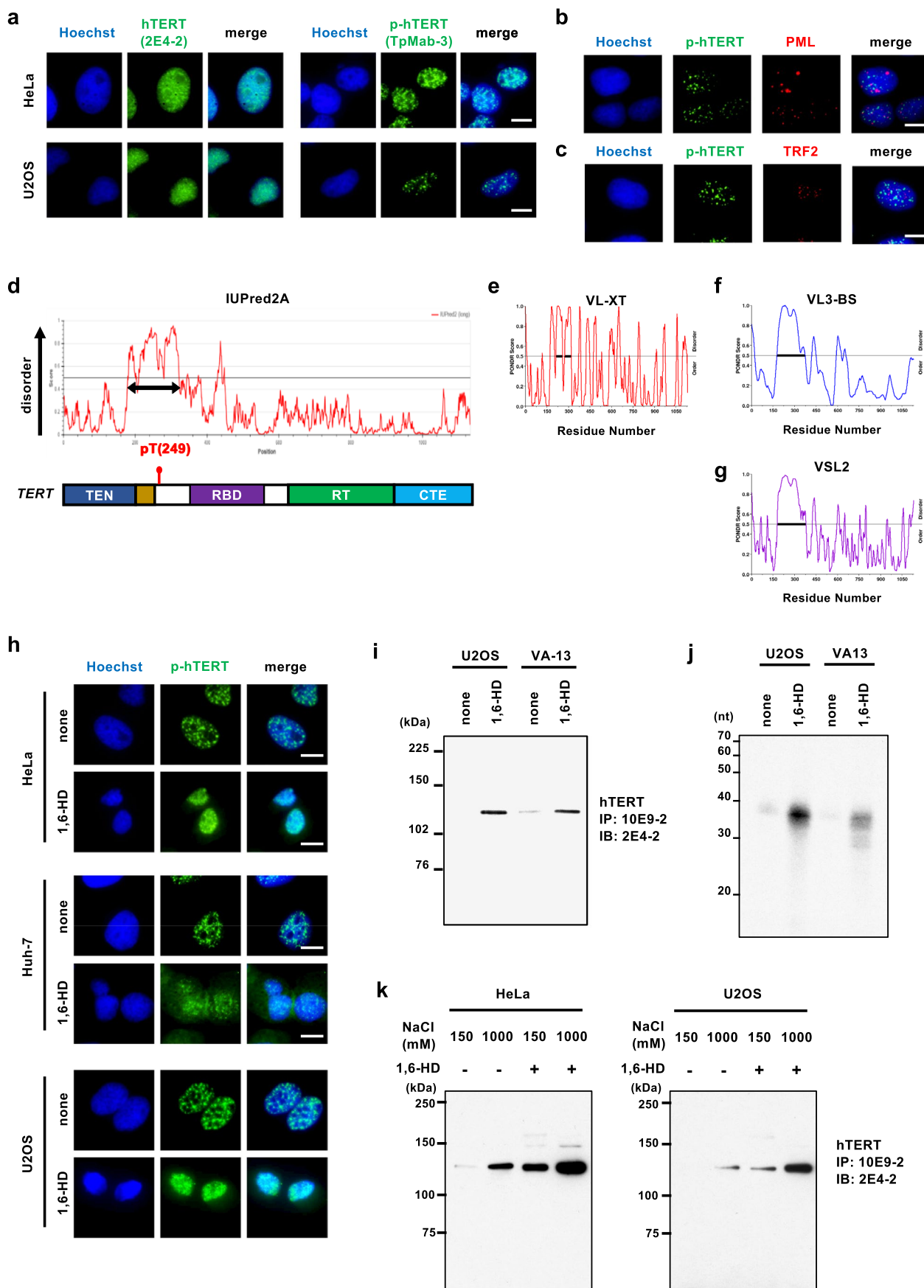
d



Extended Data Fig. 3 | See next page for caption.

Extended Data Fig. 3 | RdRP activity of hTERT alternative splicing variants.
a, Schematic diagram of hTERT alternative splicing (AS) variants. Arrows depict locations of primers used for quantitative RT-PCR analysis. **b**, Determination of hTERT AS variant levels by quantitative RT-PCR analysis ($n = 3$ independent experiments per group). Data are presented as mean \pm SD. N.D., not detected.

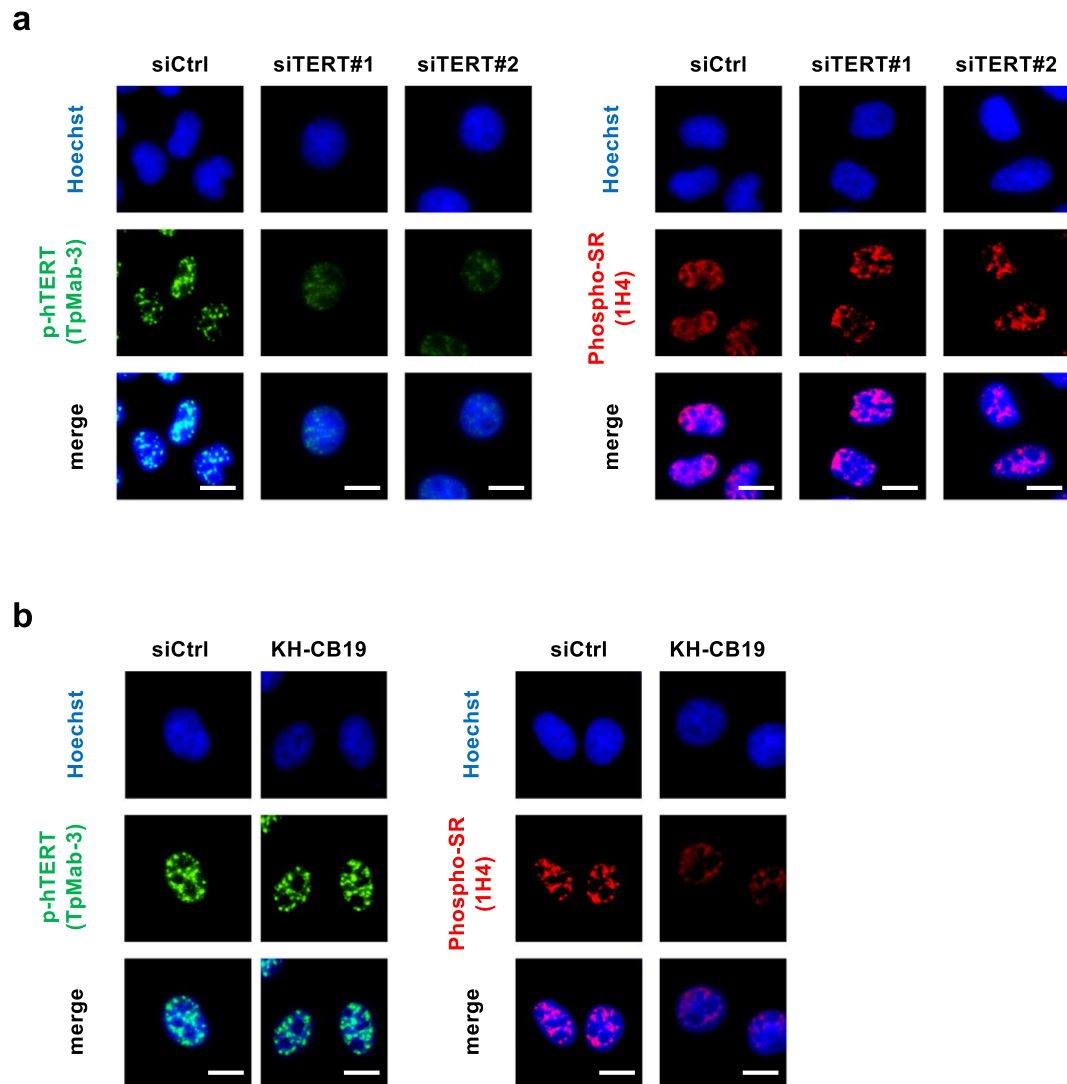
c, Detection of recombinant proteins of AS variants purified by a baculovirus expression system. * indicates migration of full-length hTERT or AS variants. **d**, IP-RdRP assay using recombinant AS variant proteins. Experiments were repeated three times (for **c**, **d**) with similar results. Source numerical data and unprocessed blots are available in source data.



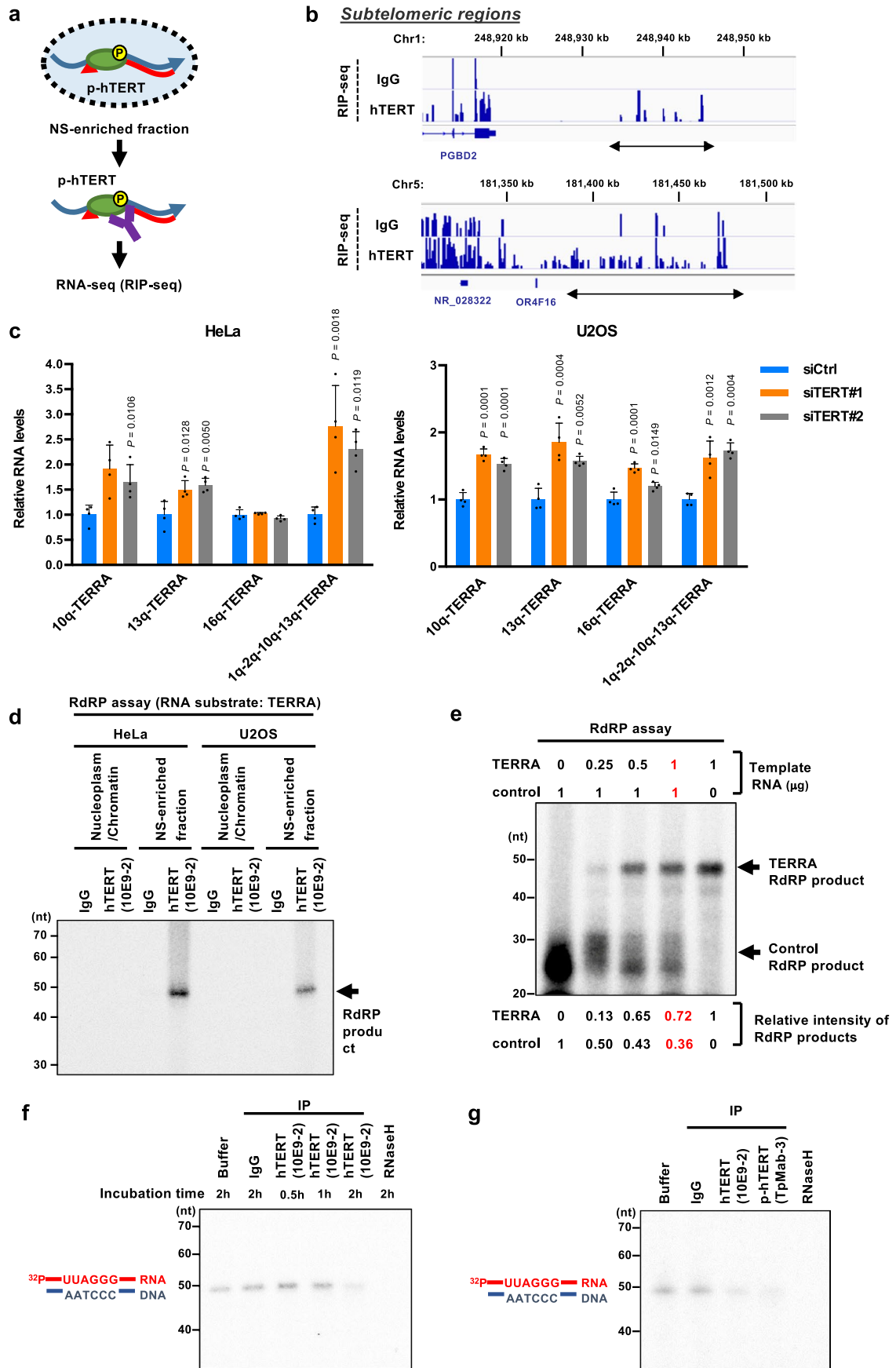
Extended Data Fig. 4 | See next page for caption.

Extended Data Fig. 4 | hTERT undergoing liquid-liquid phase separation in ALT cells. **a**, IIF imaging of hTERT (2E4-2) and p-hTERT (TpMab-3) in HeLa and U2OS cells. Scale bar, 10 μm . **b, c**, Multicolor immunofluorescence imaging of p-hTERT and PML (**b**) or TRF2 (**c**) in U2OS cells. TEN, telomerase essential N-terminal domain; RBD, RNA-binding domain; RT, reverse transcriptase domain; CTE, C-terminal extension. Scale bar, 10 μm . **d-g**, Prediction of disorder regions on hTERT protein using the IUPred2A web interface (**d**) and the PONDR predictor VL-XT (**e**), VL3-BS (**f**), or VSL2 (**g**). The bold lines show putative disorder

regions. **h**, IIF imaging of p-hTERT in HeLa, Huh-7, and U2OS cells disrupting LLPS with 10% 1,6-HD for 5 min. Scale bar, 10 μm . **i, j**, Detection of endogenous hTERT proteins (**i**) and RdRP activity (**j**) in the cells inhibiting LLPS with 1,6-HD. The 10E9-2 and 2E4-2 clones are antibodies for immunoprecipitation and immunoblotting of hTERT, respectively. **k**, Detection of endogenous hTERT protein under conditions for inhibiting LLPS (1,6-HD treatment and lysis with 150 or 1000 mM NaCl). Experiments were repeated three times (for **a, h-k**) and twice (for **b, c**) with similar results. Source unprocessed blots are available in source data.



Extended Data Fig. 5 | Specificity of an anti-p-hTERT antibody (TpMab-3). a, b, IIF imaging of p-hTERT (TpMab-3) and phospho-SR proteins (1H4) in HeLa cells treated with siRNAs specific for hTERT (a) and a CLK1 inhibitor (KH-CB19) (b). Experiments were repeated twice with similar results. Scale bar, 10 μ m.

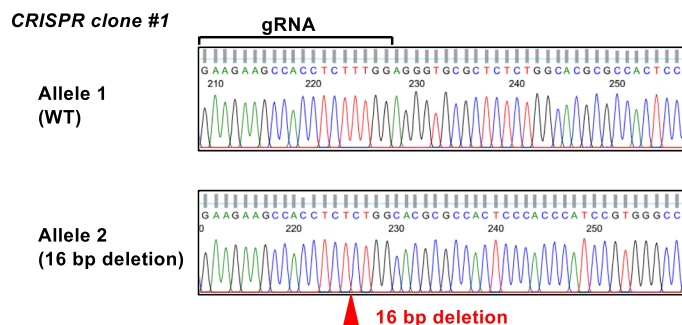


Extended Data Fig. 6 | See next page for caption.

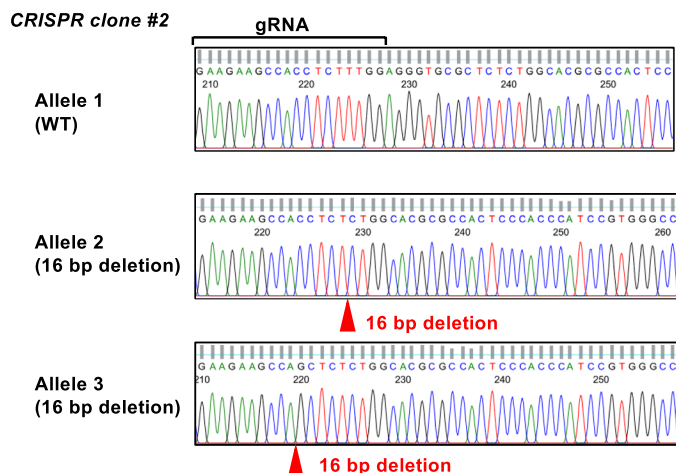
Extended Data Fig. 6 | Association between hTERT and TERRA RNAs and RdRP activity of p-hTERT against TERRA RNAs. a, Scheme of hTERT RIP-seq, which analyzed RNAs co-immunoprecipitated with hTERT using an anti-hTERT antibody (10E9-2) from nuclear speckle (NS)-enriched fraction. **b**, RIP-seq data of hTERT purified from nuclear speckles. Arrows show reads mapped to subtelomeric regions. **c**, Quantitative RT-PCR analysis of TERRA RNAs from different subtelomeric regions in hTERT knockdown HeLa and U2OS cells (n = 4 independent experiments per group). Data are presented as mean \pm SD. One-way ANOVA method with Dunnett correction for multiple comparisons between control (siCtrl) and other groups. **d**, RdRP activity of hTERT purified from nuclear

speckles against a synthetic TERRA RNA template. **e**, IP-RdRP assay using hTERT proteins immunoprecipitated with an anti-hTERT antibody (10E9-2) from the HeLa cells. A mixture of two RNA templates, control DN3AS and 5'-(CCUAAC)₈-3' for TERRA, was used for the IP-RdRP assay. **f, g**, *In vitro* R-loop degradation assay using hTERT (**f**) and p-hTERT (**g**) complex immunoprecipitated from the NS-enriched fraction and 5'-³²P-labeled TERRA RNA:DNA hybrids. RNase H is a positive control to digest RNA:DNA hybrids. Experiments were repeated three times (for **d, f**) and twice (for **e, g**) with similar results. Source numerical data and unprocessed blots are available in source data.

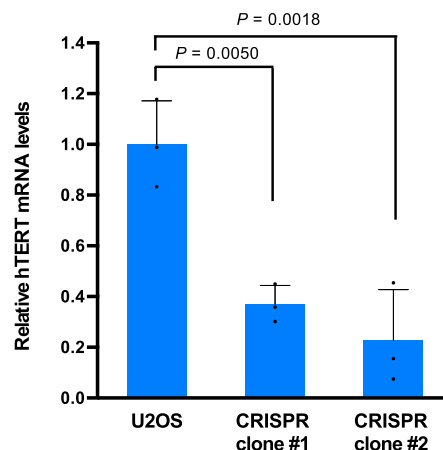
a



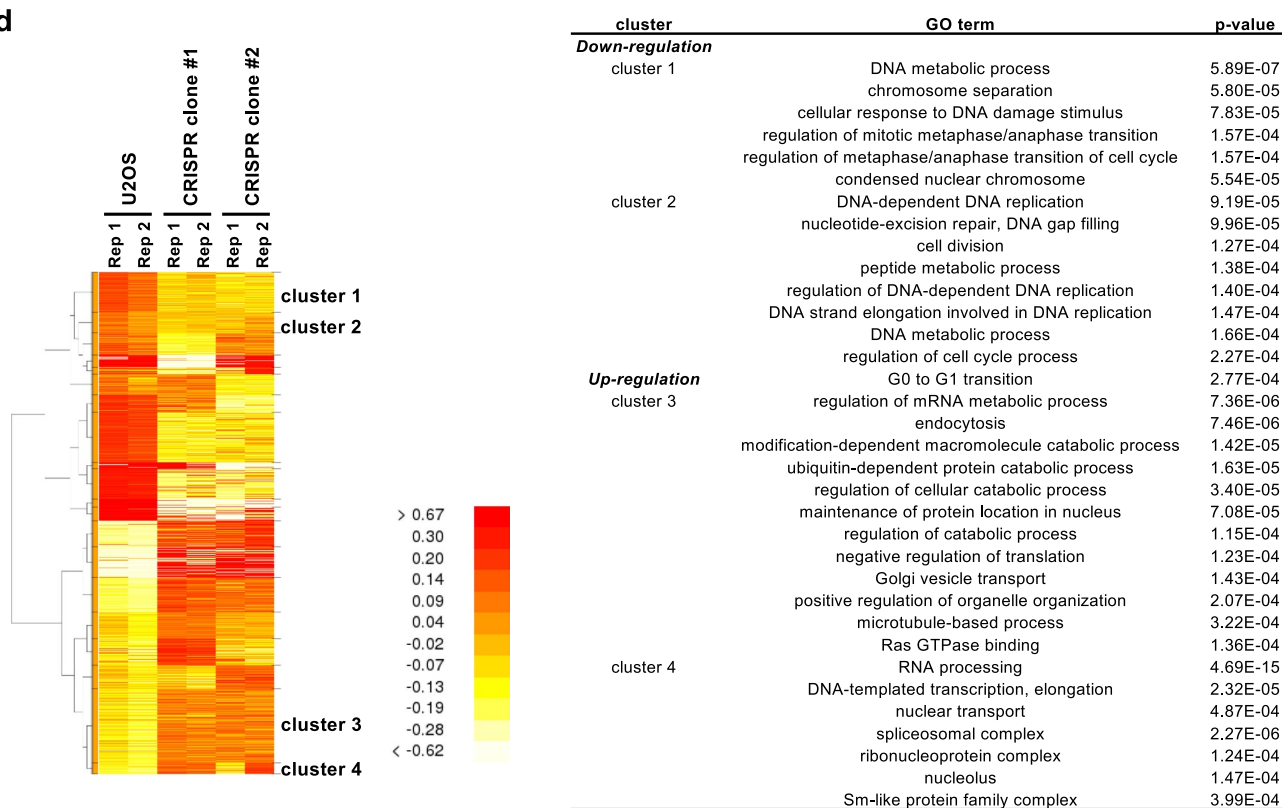
b



c



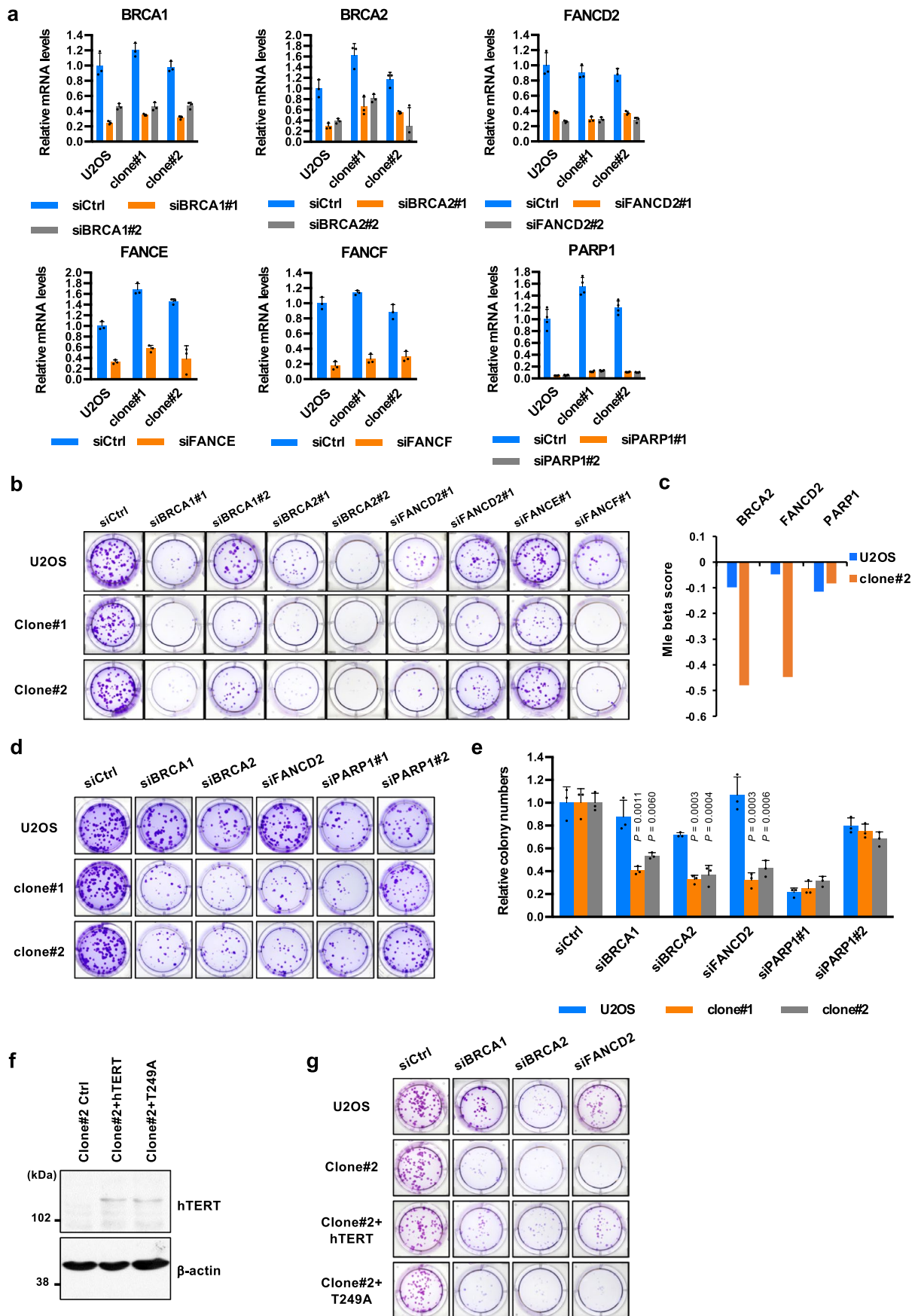
d



Extended Data Fig. 7 | See next page for caption.

Extended Data Fig. 7 | Establishment of hTERT-CRISPR clones. a, b, Sanger sequencing for the hTERT-CRISPR clones #1 (a) and #2 (b). Black lines and red arrowheads indicate the gRNA sequence and deletion regions, respectively. **c,** Determination of hTERT mRNA levels in hTERT-CRISPR clones by quantitative RT-PCR analysis ($n = 3$ independent experiments per group). Data are presented

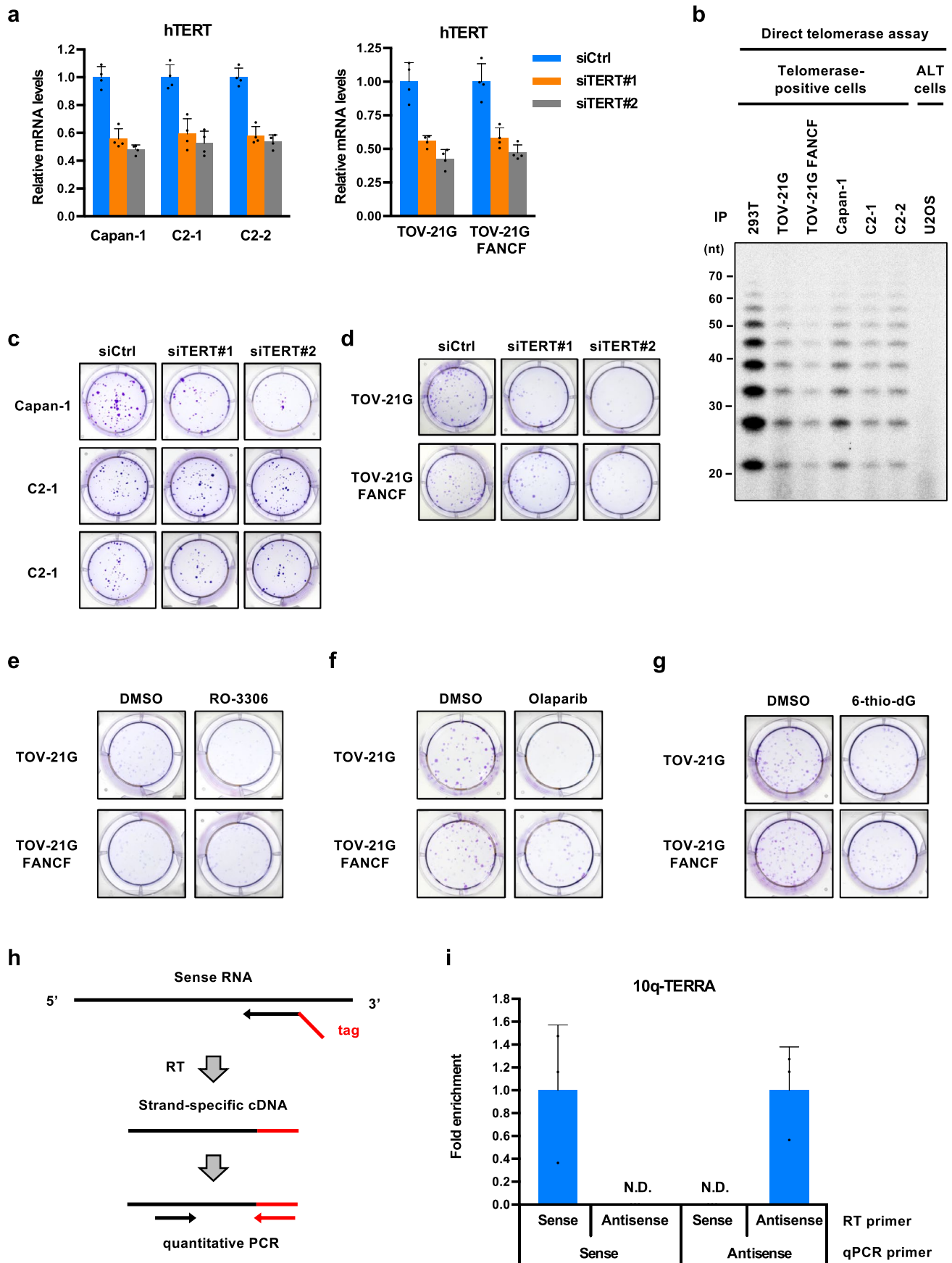
as mean \pm SD. One-way ANOVA method with Dunnett correction for multiple comparisons between control (U2OS) and other groups. **d,** Clustering and GO analyses of genes differentially expressed in hTERT-CRISPR clones. The p -values were calculated by MBCluster.Seq package. Source numerical data are available in source data.



Extended Data Fig. 8 | See next page for caption.

Extended Data Fig. 8 | Effects of FANC/BRCA knockdown and PARP1 inhibition in hTERT-CRISPR clones. **a**, Knockdown efficiencies of siRNAs specific for FANC/BRCA genes in hTERT-CRISPR clones (n = 3 independent experiments per group). **b**, The representative images of colony formation assay using hTERT-CRISPR clones transfected with siRNAs specific for FANC/BRCA genes. **c**, The MLE beta essentiality scores for FANC/BRCA and PARP1 genes generated from MAGeCK algorithm. **d**, **e**, The representative images (**d**) and colony counting (**e**) of colony formation assay using hTERT-CRISPR clones with

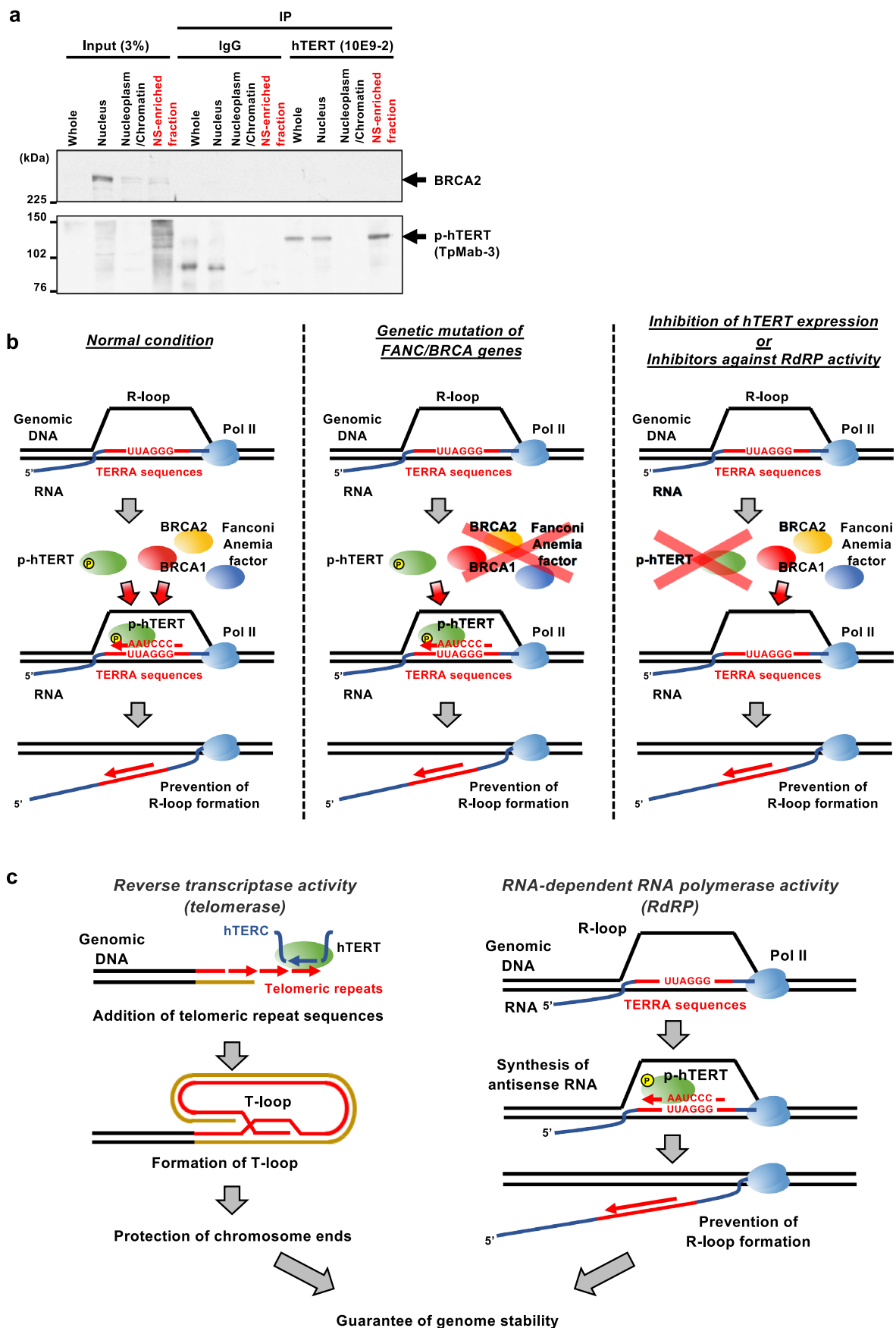
FANC/BRCA and PARP1 knockdowns (n = 3 independent experiments per group). **f**, **g**, Detection of hTERT proteins (**f**) and the representative images of colony formation assay (**g**) using hTERT-CRISPR clones overexpressing a wild-type hTERT or a T249A mutant. Data are presented as mean \pm SD (for **a**, **e**). One-way ANOVA method with Dunnett correction for multiple comparisons between control and other groups (**e**). Experiments were repeated twice with similar results (for **f**). Source numerical data and unprocessed blots are available in source data.



Extended Data Fig. 9 | See next page for caption.

Extended Data Fig. 9 | Effects of hTERT knockdown in cells lacking FANC/BRCA genes. **a**, Knockdown efficiencies of siRNAs specific for hTERT in Capan-1 and TOV-21G cell clones corrected for BRCA2 and FANCF deficiencies (n = 4 independent experiments per group). **b**, Direct telomerase assay using hTERT proteins immunoprecipitated from the indicated cells. **c-g**, The representative images of colony formation assay using these revertant clones. **h**, Schematic diagram of a strand-specific RT-PCR. DRIP RNAs were subjected to quantitative

RT-PCR (qRT-PCR) analysis with strand-specific primers with a tag sequence. **i**, qRT-PCR analysis of DRIP RNAs using tagged primers specific for sense or antisense strand TERRA RNAs (n = 3 independent experiments per group). Strand-specific qPCR primers only recognize each strand-specific cDNA. Data are presented as mean \pm SD (for **a**, **i**). Experiments were repeated twice with similar results (for **b**). Source numerical data and unprocessed blots are available in source data.



Extended Data Fig. 10 | See next page for caption.

Extended Data Fig. 10 | Maintenance of R-loop structures by p-hTERT and FANC/BRCA proteins. **a**, Immunoblotting for BRCA2 in proteins co-immunoprecipitated with hTERT from the indicated biochemical fractions. Experiments were repeated three times with similar results. **b**, Model of maintenance of R-loop structures by p-hTERT and FANC/BRCA proteins. **c**, Model of different roles of hTERT in regulation of genome stability. hTERT elongates telomeres as the catalytic enzyme of telomerase. The 3' telomeric overhangs invades into the telomere duplex and forms a small loop at the chromosome

ends, called T-loop structure, which protects the end of linear chromosomes from degradation, fusion, and recombination. On the other hand, hTERT binds to TERRA sequences of the nascent RNA transcripts and synthesizes antisense RNAs through RdRP activity. The RdRP reaction converts RNA:DNA hybrids of R-loops to dsRNAs, preventing R-loop formation. hTERT guarantees genome stability by the two enzymatic activities. Source unprocessed blots are available in source data.

Reporting Summary

Nature Portfolio wishes to improve the reproducibility of the work that we publish. This form provides structure for consistency and transparency in reporting. For further information on Nature Portfolio policies, see our [Editorial Policies](#) and the [Editorial Policy Checklist](#).

Statistics

For all statistical analyses, confirm that the following items are present in the figure legend, table legend, main text, or Methods section.

n/a | Confirmed

- The exact sample size (n) for each experimental group/condition, given as a discrete number and unit of measurement
- A statement on whether measurements were taken from distinct samples or whether the same sample was measured repeatedly
- The statistical test(s) used AND whether they are one- or two-sided
Only common tests should be described solely by name; describe more complex techniques in the Methods section.
- A description of all covariates tested
- A description of any assumptions or corrections, such as tests of normality and adjustment for multiple comparisons
- A full description of the statistical parameters including central tendency (e.g. means) or other basic estimates (e.g. regression coefficient) AND variation (e.g. standard deviation) or associated estimates of uncertainty (e.g. confidence intervals)
- For null hypothesis testing, the test statistic (e.g. F , t , r) with confidence intervals, effect sizes, degrees of freedom and P value noted
Give P values as exact values whenever suitable.
- For Bayesian analysis, information on the choice of priors and Markov chain Monte Carlo settings
- For hierarchical and complex designs, identification of the appropriate level for tests and full reporting of outcomes
- Estimates of effect sizes (e.g. Cohen's d , Pearson's r), indicating how they were calculated

Our web collection on [statistics for biologists](#) contains articles on many of the points above.

Software and code

Policy information about [availability of computer code](#)

Data collection

No software was used.

Data analysis

The following software was used to analyse the data:

- Mageck algorithm (Li et al. 2014)
- Prism version 7.03 (GraphPad Software)
- Image J version 1.52a
- Trim Galore! (version 0.6.4_dev)
- Trimmomatic (version 0.39)
- cutadapt (version 2.10)
- STAR (version 2.7.9a)
- featureCounts (version 2.0.1)
- DESeq2 package (version 1.20.0)
- MBCluster.Seq package (Si et al. 2014)
- clusterProfiler package (Yu et al. 2012)

For manuscripts utilizing custom algorithms or software that are central to the research but not yet described in published literature, software must be made available to editors and reviewers. We strongly encourage code deposition in a community repository (e.g. GitHub). See the Nature Portfolio [guidelines for submitting code & software](#) for further information.

Data

Policy information about [availability of data](#)

All manuscripts must include a [data availability statement](#). This statement should provide the following information, where applicable:

- Accession codes, unique identifiers, or web links for publicly available datasets
- A description of any restrictions on data availability
- For clinical datasets or third party data, please ensure that the statement adheres to our [policy](#)

All sequencing datasets have been deposited at the Gene Expression Omnibus (GEO) with accession codes GSE226966 and GSE226994. All the data supporting the findings of this study are available within the article and its supplementary information files.

Human research participants

Policy information about [studies involving human research participants and Sex and Gender in Research](#).

Reporting on sex and gender	Not applicable
Population characteristics	Not applicable
Recruitment	Not applicable
Ethics oversight	Not applicable

Note that full information on the approval of the study protocol must also be provided in the manuscript.

Field-specific reporting

Please select the one below that is the best fit for your research. If you are not sure, read the appropriate sections before making your selection.

Life sciences Behavioural & social sciences Ecological, evolutionary & environmental sciences

For a reference copy of the document with all sections, see [nature.com/documents/nr-reporting-summary-flat.pdf](https://www.nature.com/documents/nr-reporting-summary-flat.pdf)

Life sciences study design

All studies must disclose on these points even when the disclosure is negative.

Sample size	Sample size was based on experimental feasibility, sample availability, and N necessary to obtain definitive results.
Data exclusions	No data were excluded from our study.
Replication	All the biological experiments were repeated three times or twice and reproduced.
Randomization	Mice were assigned randomly to experimental and control groups for xenotransplantation. For experiments using culture cells, randomization is not relevant as all experiments were performed using the same experimental conditions.
Blinding	The investigators were not blinded, since experiments were performed by the same investigator. However, all experiments were independently performed multiple times. All results are based on quantitative and objective measures.

Reporting for specific materials, systems and methods

We require information from authors about some types of materials, experimental systems and methods used in many studies. Here, indicate whether each material, system or method listed is relevant to your study. If you are not sure if a list item applies to your research, read the appropriate section before selecting a response.

Eukaryotic cell lines

Policy information about [cell lines and Sex and Gender in Research](#)

Cell line source(s)	<p>The following cell lines were purchased: VA-13 (RCB0251, RIKEN BRC), Saos-2 (RCB0428, RIKEN BRC), HeLa (CVCL_0030, ATCC), Huh-7 (JCRB0403, JCRB Cell Bank), TOV-21G (CVCL_3613, ATCC), Capan-1 (HTB-79, ATCC), HEK-293T (293T) (CVCL_0063, ATCC).</p> <p>The FANCF transduced human ovarian cancer cell line TOV-21G FANCF and the BRCA2-restored Capan-1 clones (C2-1 and C2-2) were previously generated in house: TOV-21G FANCF (Taniguchi et al. 2003), The BRCA2-restored Capan-1 clones (C2-1 and C2-2) (Sakai et al. 2008).</p>
Authentication	The cell lines purchased were verified by the commercial supplier. All cell lines were authenticated in our lab by morphological examination using microscope.
Mycoplasma contamination	Cell lines were routinely tested and confirmed to be free of Mycoplasma contamination.
Commonly misidentified lines (See ICLAC register)	No commonly misidentified cell lines were used.

Animals and other research organisms

Policy information about [studies involving animals](#); [ARRIVE guidelines](#) recommended for reporting animal research, and [Sex and Gender in Research](#)

Laboratory animals	Xenotransplantation of human cell lines was performed in NOD/SCID mice. Generation of antibody was performed in BALB/c mice. Experimental mice were typically observed for 3-5 weeks. All mice were closely monitored by investigators and facility technicians every two or three days.
Wild animals	The study did not involve wild animals.
Reporting on sex	Six-week-old male mice were used as recipients for xenotransplantation.
Field-collected samples	The study did not involve samples collected from the field.
Ethics oversight	All animal experiments were performed in accordance with the study protocols approved by the Animal Care and Use Committee of Kanazawa University and Tohoku University.

Note that full information on the approval of the study protocol must also be provided in the manuscript.